Geosci. Model Dev. Discuss., doi:10.5194/gmd-2016-131, 2016
Manuscript under review for journal Geosci. Model Dev.
Published: 7 June 2016

Geoscientific Model Development Discussions
Open Access
EGU

Ozone air quality simulations with WRF-Chem (v3.5.1) over Europe: Model evaluation and chemical mechanism comparison

Kathleen A. Mar[1], Narendra Ojha[2], Andrea Pozzer[2], and Tim M. Butler[1]

[1]Institute for Advanced Sustainability Studies, Potsdam, Germany
[2]Atmospheric Chemistry Department, Max Planck Institute for Chemistry, Mainz, Germany

Correspondence to: K. A. Mar (Kathleen.Mar@iass-potsdam.de)

Abstract. We present an evaluation of the online regional model WRF-Chem over Europe with a focus on ground-level ozone (O_3) and nitrogen oxides (NO_x). The model performance is evaluated for two chemical mechanisms, MOZART-4 and RADM2, for year-long simulations. Model-predicted surface meteorological variables (e.g., temperature, wind speed and direction) compared well overall with surface-based observations, consistent with other WRF studies. WRF-Chem simulations employing MOZART-4 as well as RADM2 chemistry were found to reproduce the observed spatial variability in surface ozone over Europe. However, the absolute O_3 concentrations predicted by the two chemical mechanisms were found to be quite different, with MOZART-4 predicting O_3 concentrations up to 20 $\mu g\,m^{-3}$ greater than RADM2 in summer. Compared to observations, MOZART-4 chemistry overpredicted O_3 concentrations for most of Europe in the summer and fall, with a summertime domain-wide mean bias of +10 $\mu g\,m^{-3}$ against observations from the AirBase network. In contrast, RADM2 chemistry generally led to an underestimation of O_3 over the European domain in all seasons. We found that the use of the MOZART-4 mechanism, evaluated here for the first time for a European domain, led to lower absolute biases than RADM2 when compared to ground-based observations. The two mechanisms show relatively similar behavior for NO_x, with both MOZART-4 and RADM2 resulting in a slight underestimation of NO_x compared to surface observations. Further investigation into the differences between the two mechanisms revealed that the net midday photochemical production rate of O_3 in summer is higher for MOZART-4 than for RADM2 for most of the domain. The largest differences in O_3 production can be seen over Germany, where net O_3 production in MOZART-4 is seen to be higher than in RADM2 by 1.8 $ppb\,hr^{-1}$ (3.6 $\mu g\,m^{-3}\,hr^{-1}$) or more. We also show that, while the two mechanisms exhibit similar NO_x-sensitivity, RADM2 is approximately twice as sensitive to increases in anthropogenic VOC emissions as MOZART-4. Ad-

Geosci. Model Dev. Discuss., doi:10.5194/gmd-2016-131, 2016
Manuscript under review for journal Geosci. Model Dev.
Published: 7 June 2016

Geoscientific Model Development Discussions
Open Access
EGU

ditionally, we found that differences in reaction rate constants for inorganic gas phase chemistry in MOZART-4 vs. RADM2 accounted for a difference of 8 $\mu g\,m^{-3}$ in O_3 predicted by the two mechanisms, whereas differences in deposition and photolysis schemes explained smaller differences in in O_3. Our results highlight the strong dependence of modeled surface O_3 over Europe on the choice of gas phase chemical mechanism, which we discuss in the context of overall uncertainties in prediction of ground-level O_3 and its associated health impacts (via the health-related metrics MDA8 and SOMO35).

Geosci. Model Dev. Discuss., doi:10.5194/gmd-2016-131, 2016
Manuscript under review for journal Geosci. Model Dev.
Published: 7 June 2016

Geoscientific Model Development Discussions
Open Access
EGU

1 Introduction

Tropospheric ozone (O_3) is an air pollutant with adverse effects on human and ecosystem health as well as a short-lived climate forcer with a significant warming effect (e.g., Monks et al., 2015; Stevenson et al., 2013; WHO, 2003). In Europe, ozone pollution remains a problem: the European Environmental Agency reports that between 2010 and 2012, 98% of Europe's urban population was exposed to O_3 levels in exceedance of the WHO air quality guideline (EEA, 2014), leading to more than 6000 premature deaths annually (Lelieveld et al., 2015). This is despite the fact that European emissions of ozone precursors, in particular nitrogen oxides (NO_x) and volatile organic compounds (VOCs), have decreased significantly since 1990. The persistance of unhealthy levels of ozone in Europe can be attributed to increases in hemispheric background ozone (Wilson et al., 2012) as well as the non-linear relationship between O_3 and levels of precursor species NO_x and VOC (EEA, 2014).

Air quality models are employed to understand the drivers of air pollution at a regional scale and to evaluate the roles of and interactions between emissions, meteorology and chemistry. These models fall into two broad categories: offline Chemistry-Transport Models (CTMs), in which meteorology is calculated separately from model chemistry, and "online" models, the category to which WRF-Chem belongs, in which the meteorology and chemistry are coupled, meaning they are solved together in a physically consistent manner (e.g., Zhang, 2008). The meteorology and chemistry components in WRF-Chem use the same horizontal and vertical grids and same timestep, eliminating the need for temporal interpolation (e.g., Grell et al., 2004, 2005).

Air quality modeling studies over the European region have predominantly utilized CTMs, examples of which include EMEP (Simpson et al., 2012), CHIMERE (Terrenoire et al., 2015), and LOTOS-EUROS (Schaap et al., 2008). Recently, application of WRF-Chem over Europe has increased (e.g., Solazzo et al., 2012a, b; Tuccella et al., 2012; Zhang et al., 2013a, b; Baklanov et al., 2014). However, only a limited number of studies dedicated to the evaluation of WRF-Chem simulated meteorology and chemistry for the European domain are available in the literature. The study of Tuccella et al. (2012) evaluated the performance of WRF-Chem using the RADM2 chemical mechanism by comparing domain-wide average values against observations of meteorology and chemistry. However, an evaluation of the spatial distribution of model-simulated meteorology and trace gases is missing. This type of spatial information is extremely pertinent for air quality management applications, where model performance at a national scale can become more relevant than performance metrics applied to the whole of Europe; this information gets lost when only comparing quantitities that have been averaged over the entire domain. Additionally, Tuccella et al. (2012) utilized time-invariant chemical boundary conditions, which the authors suggested misrepresented the seasonal changes in the intercontinental transport (Tuccella et al., 2012). In addition to the study of Tuccella et al. (2012), Zhang et al. (2013b) evaluated the performance WRF-Chem-MADRID (Zhang et al., 2010), an unofficial version of WRF-Chem coupled to the Model of Aerosol Dynamics, Reaction,

Geosci. Model Dev. Discuss., doi:10.5194/gmd-2016-131, 2016
Manuscript under review for journal Geosci. Model Dev.
Published: 7 June 2016

Geoscientific Model Development Discussions
Open Access
EGU

Ionization, and Dissolution (MADRID), over Europe for the month of July 2001, employing the gas-phase mechanism CB05 (Yarwood et al., 2005). This detailed study provides a valuable reference for comparison to the present work, but their simulations are only for one month, rather than the complete seasonal cycle.

Several groups contributed WRF-Chem simulations to the AQMEII project (phase 1 and phase 2) for the European domain (Solazzo et al., 2012b; Im et al., 2015). In AQMEII phase 1, two different WRF-Chem simulations were part of the model ensemble for Europe, but evaluation of model performance for ozone focused on evaluation of the ensemble (Solazzo et al., 2012b), rather than on individual members. In fact, in the analysis of Solazzo et al. (2012b), individual models were anonymized, meaning the performance statistics for the WRF-Chem ensemble members are not explicitly presented. The evaluation of model performance with respect to ozone in AQMEII phase 2 (Im et al., 2015) provides more information on the model performance of the contributing WRF-Chem ensemble members for the European domain. In AQMEII phase 2, seven different WRF-Chem runs were part of the ensemble. Of these seven simulations, four of them used the gas phase chemical mechanism RADM2 (Stockwell et al., 1990), two used the mechanism CBMZ (Zaveri and Peters, 1999), and one used the mechanism RACM (Stockwell et al., 1997; Geiger et al., 2003). All WRF-Chem simulations for Europe in AQMEII phase 2 tended to underestimate ozone concentrations, with annual average normalized mean bias ranging from -1.6 to -15.8 %, depending on the ensemble member.

The purpose of the present study is to perform a detailed evaluation of meteorology and gas phase chemistry simulated by WRF-Chem, including the spatial and seasonal variations over a full year seasonal cycle using time-varying chemical boundary conditions. This evaluation is performed for two different gas phase chemical mechanisms within WRF-Chem, MOZART-4 (Emmons et al., 2010) and RADM2 (Stockwell et al., 1990). As discussed above, the RADM2 mechanism has been popularly used in WRF-Chem for simulation over Europe (Tuccella et al., 2012; Im et al., 2015). The MOZART-4 chemical mechanism has been widely used with WRF-Chem for regional air quality applications outside of Europe (e.g., Pfister et al., 2013; Im et al., 2015). To the authors' knowledge, however, WRF-Chem with MOZART-4 has never been applied and evaluated over a European domain.

The simultaneous evaluation of WRF-Chem with two different chemical mechanisms further allows us to evaluate the sensitivity of O_3 and NO_x to the choice of chemical mechanism in a setup where the differences in model physics and other parameters are minimized. This is in contrast to the study of Im et al. (2015), where the various WRF-Chem ensemble members also used different schemes for model physics. Coates and Butler (2015) recently investigated the sensitivity of the production of odd oxygen (O_x, a proxy for production of O_3) to the choice of chemical mechanism using a box model, and found that choice of chemical mechanism led to differences in O_3 concentrations on the order of 10 ppb under idealized conditions, although differences between the MOZART-4

Geosci. Model Dev. Discuss., doi:10.5194/gmd-2016-131, 2016
Manuscript under review for journal Geosci. Model Dev.
Published: 7 June 2016

and RADM2 chemical mechanisms tended to be closer to 5 ppb. In another box model study, Knote et al. (2015) investigated the sensitivity of O_3, NO_x, and other radicals to the different gas-phase chemical mechanisms used in the models that contributed to the AQMEII phase-2 intercomparison project. Knote et al. (2015) found that the choice of chemical mechanism is responsible for a 5% uncertainty in predicted O_3 concentrations and a 25% uncertainty in predicted NO_x concentrations.

The present study builds on the work of Coates and Butler (2015) and Knote et al. (2015) by comparing two chemical mechanisms within an online coupled regional air quality model. The use of WRF-Chem provides an advantage in that it is compatible with multiple different chemical mechanisms, allowing us to test the effect of different chemistry with minimal confounding factors due to differences in model physics, etc. Furthermore, the use of an online regional model rather than a box model allows us to examine the sensitivity of model-predicted concentrations to the choice of chemical mechanism under more realistic conditions, in which variations in meteorology and dynamics is fully included. Parameters such as radiation are allowed to vary realistically, and different chemical regimes (NO_x- vs. VOC-limited) are present (e.g., in different seasons and in different parts of the model domain).

Chemical mechanism comparisons have also been undertaken previously using 3-D regional air quality models, though the majority have focused on comparing the SAPRC-99 mechanism (Carter, 1990) with versions of the Carbon Bond mechanism (Gery et al., 1989) over a U.S. domain (Luecken et al., 2008; Faraji et al., 2008; Yarwood et al., 2003; Zhang et al., 2012). Two additional studies have compared versions of the RACM mechanism with RADM2 (Mallet and Sportisse, 2006) and CB05 (Kim et al., 2010) using the model Polyphemus (Mallet et al., 2007) for a European domain. Typically, these studies found that simulations using two different chemical mechanisms led to differences in O_3 on the order of 5-10 ppb (Luecken et al., 2008; Zhang et al., 2012; Mallet and Sportisse, 2006; Kim et al., 2010), although extreme differences of 30-40 ppb were observed between SAPRC-99 and CB-IV mechanisms when simulating high ozone episodes (Faraji et al., 2008; Yarwood et al., 2003).

In this paper, the model configuration, including emissions and initial and boundary conditions, is described in Section 2. A description of observational datasets for meteorology and chemistry and the evaluation methodology is provided in Section 3. Results for the model evaluation and intercomparison of two chemical are presented in Section 4 followed by a summary and concluding remarks in Section 5.

Geosci. Model Dev. Discuss., doi:10.5194/gmd-2016-131, 2016
Manuscript under review for journal Geosci. Model Dev.
Published: 7 June 2016

Geoscientific Model Development Discussions
Open Access
EGU

2 Model Description and Setup

2.1 WRF-Chem

This study utilizes the Weather Research and Forecasting with Chemistry (WRF-Chem) model (http://ruc.noaa.gov/wrf/WG11) version 3.5.1. WRF-Chem has been developed collaboratively by NOAA, DOE/PNNL, NCAR and other research institutes (https://www2.acd.ucar.edu/wrf-chem).

We defined our simulation domain on the Lambert projection. The model domain is centered at 15° E, 52° N, and covers nearly the entire European region. The horizontal resolution is chosen to be 45 $\mathrm{km} \times 45\,\mathrm{km}$. The model domain has 115 and 100 grid points in the west-east and south-north directions respectively.

We have used 35 vertical levels in the model starting from surface to 10 hPa. The lowest model level corresponds to an approximate altitude of 50 m above the surface. Tests have shown that surface layer concentrations in this configuration are effectively the same as when the lowest model level is at a height of 14 m, but with no urban surface physics scheme (the urban physics scheme is incompatible with a 14-m model level). Geographical data including terrain height, soil properties, albedo, etc. are interpolated primarily from USGS (United States Geological Survey data (Wang et al., 2014)) at 30 sec resolution. The land use classification has been interpolated from the CORINE data (EEA, 2012) at 250 m resolution, which was then mapped to the USGS land use classes used by WRF (see Kuik et al., 2016).

Model simulations are conducted for the period of 23 December 2006 to 31 December 2007. The first week of output was treated as model spin up and has been discarded. The instantaneous model output, stored every hour, has been used for the analysis. The different options used in this study to parametrize the atmospheric processes are listed in Table 1. A namelist is available in the Supplementary Material.

The initial and lateral boundary conditions for the meteorological fields were provided from the ERA-interim reanalysis dataset available from ECMWF (http://www.ecmwf.int/en/research/climate-reanalysis/era-interim). This data is available every 6 hours with a spatial resolution of approximately 80 km (T255 spectral). In order to limit the errors in the WRF simulated meteorology the Four Dimensional Data Assimilation (FDDA) has been applied. In the FDDA, temperature is nudged at all the vertical levels with a nudging coefficient of 0.0003. The horizontal winds are nudged at all the vertical levels, except within the PBL, with the nudging coefficient of 0.0003. Sensitivity studies performed showed that nudging of water vapor highly suppressed the precipitation over Europe in a manner inconsistent with observations. As such, water vapor is not nudged in our simulations. This also follows the approach of, e.g., Miguez-Macho et al. (2004) and Stegehuis et al. (2014). The nudging coefficients for temperature and winds have been chosen following previous studies (Stauffer et al., 1991; Liu et al., 2012). The time step for the simulations has been set at 180 s.

Geosci. Model Dev. Discuss., doi:10.5194/gmd-2016-131, 2016
Manuscript under review for journal Geosci. Model Dev.
Published: 7 June 2016

Initial and boundary conditions for chemical fields in WRF-Chem are used from the MOZART-4/GEOS5 simulations (http://www.acd.ucar.edu/wrf-chem/mozart.shtml), with a horizontal resolution of $1.9° \times 2.5°$and 56 pressure levels. MOZART-4/GEOS-5 simulations use meteorology from the NASA GMAO GEOS-5 model and emissions based on ARCTAS inventory (http://www.cgrer.uiowa.edu/arctas/emission.html).

2.2 Emissions

Anthropogenic emissions of CO, NO_x, SO_2, NMVOCs, PM_{10}, PM_{25}, and NH_3 are used from the TNO-MACC II emission inventory for Europe (Kuenen et al., 2014), for the year 2007. These emissions are provided as yearly totals by source sector on a high-resolution ($7\,\mathrm{km} \times 7\,\mathrm{km}$) grid. The TNO-MACC II emission inventory is based on emissions reported by member countries to the European Monitoring and Evaluation Program (EMEP), which are then further refined to fill gaps and correct errors and obvious inconsistencies. Emissions are temporally disaggregated based on seasonal, weekly and diurnal cycles provided by Denier van der Gon et al. (2011); Schaap et al. (2005). These temporal profiles vary by source sector according to the SNAP (Selected Nomenclature for Sources of Air Pollution) convention. NMVOC emissions are split into modeled NMVOC species (e.g., ethane, aldehydes) based on von Schneidemesser et al. (2016). NO_x is emitted as 90% NO and 10% NO_2 by mole. Emissions are distributed into the first seven model vertical layers (the surface and the first 6 model layers above the surface) based on sectoral averages from (Bieser et al., 2011), although model runs showed little sensitivity to the distribution of emissions above the surface layer.

The model domain used in this study is larger than the European domain used in the TNO-MACC II inventory (Kuenen et al., 2014). Emissions at our domain edges were filled using the Hemispheric Transport of Air Pollution (HTAP v2.2) emission inventory for the year 2008 (http://edgar.jrc.ec.europa.eu/htap_v2/index.php). The HTAP v2 data, described in detail by Janssens-Maenhout et al. (2015), is harmonized at a spatial resolution of 0.1° x 0.1° and available with monthly time resolution. In our model simulations, no additional weekly or diurnal profiles were applied to the HTAP v2 emissions. Furthermore, all emissions from HTAP were emitted into the surface model layer. Because HTAP emissions were only used at the grid "edge," the differences in temporal and vertical resolution of emissions used for HTAP is not expected to have a significant impact on model results. An example of emissions processed for model input is shown in the Supplementary Material.

Biomass burning emissions are from the Fire Inventory from NCAR (FINN), Version 1 (Wiedinmyer et al., 2011). To avoid the double counting of emissions from agricultural burning (i.e., assuming that the FINN product captures large-scale agricultural burning), emissions of the combustion species CO, NO_x, and SO_2 from SNAP category 10 (Agriculture) in the TNO-MACC II inventory were not included in model simulations, at the suggestion of H.A.C. van der Gon (personal commu-

Geosci. Model Dev. Discuss., doi:10.5194/gmd-2016-131, 2016
Manuscript under review for journal Geosci. Model Dev.
Published: 7 June 2016

Geoscientific Model Development Discussions
Open Access
EGU

nication, 2015). Biogenic Emissions are calculated online based on weather and land use data using the Model of Emissions of Gases and Aerosols from Nature (MEGAN) (Guenther et al., 2006).

2.3 Model Chemistry

The two year-long WRF-Chem simulations performed for this study are summarized in Table 2. In the MOZART simulation, gas phase chemistry is represented by the Model for Ozone and and Related chemical Tracers, version 4 (MOZART-4) mechanism (Emmons et al., 2010). Tropospheric chemistry is represented by 81 chemical species, which participate in 38 photolysis and 159 gas-phase reactions. The MOZART-4 mechanism includes explicit representation of the NMVOCs ethane, propane, ethene, propene, methanol, isoprene, and α-pinene. Other NMVOC species are represented by lumped species based on the reactive functional groups. In the WRFV3.5.1 code, two bug fixes have been included for the MOZART-4 mechanism: the NH_3+OH rate constant has been corrected following Knote et al. (2015), and a correction has been made to treatment of the vertical mixing of MOZART-4 species (A.K. Peterson, personal communication). In the WRF-Chem simulations, we use the version of MOZART-4 coupled to the simple GOCART aerosols mechanism (Ackermann et al., 1998b), known as the MOZCART mechanism. In this paper, we limit our analysis to gas-phase species. Because of this focus, and to simplify the interpretation the mechanism intercomparison (see below), all aerosol radiative feedbacks (i.e., both direct and indirect effects) are turned off in all model simulations in this study.

In the RADM2 simulation, gas phase chemistry is represented by the second generation Regional Acid deposition Model (RADM2) (Stockwell et al., 1990). This mechanism has 63 chemical species which participate in 21 photolysis and 136 gas phase reactions. The NMVOC oxidation in RADM2 is treated in a less-explicit fashion than in MOZART, in which ethane, ethene and isoprene are the only species treated explicitly and all other NMVOCs are assigned to lumped species based on OH reactivity and molecular weight. In WRF-Chem, RADM2 is coupled to the MADE/SORGAM aerosol module, which is based on the Modal Aerosol Dynamics Model for Europe (MADE) (Binkowski and Shankar, 1995; Ackermann et al., 1998a) and Secondary Organic Aerosol Model (SORGAM) (Schell et al., 2001) . However, as noted above, in this study we focus our analysis on gas-phase chemistry.

In both the RADM2 and MOZART simulations, the chemical mechanism code was generated with the Kinetic Pre-Processor (KPP) (Damian et al., 2002; Sandu and Sander, 2006), and equations are solved using a Rosenbrock-type solver. Note that when using RADM2 chemistry, there are two different solvers available within WRF-Chem. We chose to use the KPP chemistry and Rosenbrock solver to be consistent with the MOZART runs, and also because the alternative QSSA chemistry solver has been shown to have problems representing NO_x titration (Forkel et al., 2015). In particular, the QSSA treatment of RADM2 chemistry was found to result in an under-representation fo nocturnal ozone titration for areas with high NO emissions.

Geosci. Model Dev. Discuss., doi:10.5194/gmd-2016-131, 2016
Manuscript under review for journal Geosci. Model Dev.
Published: 7 June 2016

3 Observational datasets

A summary of the observational datasets used for model evaluation can be found in Table 3.

3.1 Meteorology

Since WRF-Chem couples the meteorology simulations online with the chemistry, we begin by evaluating the modeled meteorological fields against observations which are driving the simulations of chemical fields. In this study, the WRF-Chem simulated meteorological fields are evaluated against the in situ measurements of mean sea level pressure (MSLP), 2-meter temperature (T2) and 10-meter wind speed and direction (WS10 and WD10, respectively) from the Global Weather Observation dataset provided by the British Atmospheric Data Center (BADC). We chose these meteorological variables for the evaluation as these are expected to have the most significant influence on the gas-phase chemistry, which is the main focus of this study.

3.2 Chemistry

3.2.1 EMEP Network

The EMEP observational dataset provides surface measurements of pollutant concentrations, including tropospheric ozone and its precursors, at stations chosen to be representative of regional background pollution (see, e.g., Tørseth et al., 2012). The regional focus is in keeping with the goals of the Convention on Long-range Transboundary Air Pollution (CLRTAP), under which this network is administrated.

3.2.2 AirBase Network

AirBase is the public air quality database of the European Environmental Agency (EEA), and represents a much denser network of monitoring than the EMEP network (http://www.eea.europa.eu/data-and-maps/data/airbase-the-european-air-quality-database-7). Because of the relatively coarse horizontal resolution in this model study, model output is only compared against AirBase stations that are classified as "rural background." Some AirBase stations are also part of the EMEP network; the subset of AirBase stations used in this study exclude any stations that are also part of the EMEP network (since they are already included in the evaluation against EMEP observations).

3.3 Evaluation methodology

Stations were excluded from our season-by-season analysis if the temporal coverage was less than 75%, i.e., if missing or flagged hourly (or 3-hourly) data represented more than 25% of the hourly (or 3-hourly) time series over the entire season. For sensitivity studies that consider the month of July only, stations were considered that had at least 75% temporal coverage for the month. This

Geosci. Model Dev. Discuss., doi:10.5194/gmd-2016-131, 2016
Manuscript under review for journal Geosci. Model Dev.
Published: 7 June 2016

criteria was applied for all meteorological and chemistry observations. For comparison of model output to in situ observations, the model gridcell that is closest to the latitude, longitude location of the measurement station was chosen. Statistics calculated include the mean, mean bias (MB), normalized mean bias (NMB), mean fractional bias (MFB) and the temporal correlation coefficient (r). The domain-wide statistics presented in Tables 4 - 9 were calculating by first calculating the statistical quantity hour-by-hour at each station, and then averaging these values over all times (in the season) and all stations. Definitions of calculated statistical quantities can be found in Appendix B.

From hourly concentrations of O_3, either observed or modeled, additional ozone metrics for health impacts are calculated. MDA8 is defined as the maximum daily 8-hour mean ozone, in accordance with the European Union's Air Quality Directive. Note that, for calculation of MDA8, a missing value was assigned if one or more hours of data in the 8-hour average were missing. SOMO35 is defined as the sum of MDA8 levels over 35 ppb (70 $\mu g\,m^{-3}$) over a year, in units of concentration·days, following Regional Office for Europe (2008).

$$SOMO35 = \frac{365}{N_{valid}} \sum_{iday} max(0, C_{iday} - 70\ \mu g\,m^{-3})$$

where N_{valid} is the number of valid (i.e., non-missing) daily values.

4 Results and Discussion

4.1 Evaluation of Meteorology

Table 4 shows a summary of domain-wide statistics evaluating the model simulations against observations of meteorological variables MSLP, T2, WS10 and WD10; the spatial distribution of these statistics shown in Figures 1-3 for temperature and wind variables. (Shown in Table 4 and Figures 1-3 are model output from the MOZART simulation; differences between the MOZART and RADM2 simulations are negligible, as expected based on fact that simulations were run without aerosol-radiative feedbacks.) MSLP has been reproduced over the entire European domain with a high degree of skill in every season, with negligible bias (domain-averaged NMB and MFB are zero in all seasons) and temporal correlation coefficients (r values) of 0.98 or greater (see also Figure S2 in the Supplementary Material).

The spatial distribution of seasonal average T2 in the model and observations is shown in Figure 1, along with the spatial variation in mean bias and temporal (3-hourly) correlation. Overall the spatial variability in measured T2 is found to be well-reproduced by WRF-Chem during all the seasons. The absolute values of mean biases in T2 were generally found to be lower than 1° C. Larger biases in T2 can be found in the Alps, in particular during winter, where T2 is often overpredicted by more than 1° C (Figure 1). This larger bias over mountainous regions, also found in a previous study (Zhang et al., 2013a), is likely due to the complex mountain terrain and associated unresolved

Geosci. Model Dev. Discuss., doi:10.5194/gmd-2016-131, 2016
Manuscript under review for journal Geosci. Model Dev.
Published: 7 June 2016

local dynamics. The r values are generally found to be more than 0.9 in all the seasons and show no significant geographical variation, indicating that the model is able to reproduce the hourly variations in near surface temperature. Averaged over the entire domain, the mean bias in T2 varies from -0.4 to + 0.3° C depending on the season (Table 4). varies from -0.4 to + 0.3° C depending on the season (Table 4).

The spatial variability in wind speeds, including the seasonality with strongest winds during the winter have been reproduced by the model (Figure 2). However, the model tends to overestimate winds speeds with larger biases (2 m/s or more) during the winter and fall. The regions showing greater bias in wind speed include the Alps, coastal regions, and the low-lying areas of northern Germany and Denmark (Figure 2). The temporal correlation of wind speed is generally above 0.7 in the northern half of the domain, but is lower (0.4-0.6) in the southern part of the domain, in areas in the Alps and close to the Mediterranean (Figure 2). Similar behavior for modeled wind speed is reported by Zhang et al. (2013a), who attributes the overestimation in wind speeds primarily to poor representation of surface drag exerted by unresolved topographical features, which results in model limitations in simulating circulation systems such as sea breeze and bay breeze. An overview of the statistics for wind direction is presented in Table 4, with the spatial distribution shown in Figure 3. Wind comes dominantly from the west and south, and the mean bias in wind direction is between 20 and 30 degrees depending on the season. Similar to the patterns seen for wind speed, areas with complex topography (the Alps, the Balkans, the Mediterranean coast) show the largest biases and the lowest correlations for wind direction.

Overall, we find that WRF-Chem is capable of reproducing the spatial and temporal variations in the European meteorological conditions reasonably well, in a manner consistent with previous studies (e.g. Zhang et al., 2013a).

4.2 Evaluation of Chemistry

4.2.1 Ozone

We begin the evaluation of chemistry by examining the seasonal average surface O_3 distribution over Europe from the MOZART simulation, as shown in Figure 4. Predicted surface O_3 distributions show a clear seasonality, with maximum concentrations during summer. In all seasons, surface O_3 concentrations are highest over the Mediterranean region, with values during the spring and summer greater than 110 $\mu g\,m^{-3}$. Simulated concentrations reproduce the north-south gradient in O_3 seen in the ground-based observations. Figure 5 provides another comparison of seasonal average O_3 distributions in the model vs. the observations (from both the AirBase and EMEP networks) and additionally shows the spatial distribution of MB and r, the temporal (hourly) correlation coefficient; performance statistics are shown in Table 5 (against observations from the AirBase network) and Table 6 (against observations from the EMEP network). MOZART overpredicts O_3 concentrations

Geosci. Model Dev. Discuss., doi:10.5194/gmd-2016-131, 2016
Manuscript under review for journal Geosci. Model Dev.
Published: 7 June 2016

Geoscientific Model Development Discussions
Open Access
EGU

for most of Europe in the summer and fall. In winter and spring, MOZART tends to underestimate O_3 in north-central Europe, but overestimate O_3 in southern Europe. Hourly correlation coefficents for O_3 are highest (greater than 0.6) in northern Europe (especially France, Germany, and the Benelux region) and in Spain, but are lower (with values of approximately 0.4) throughout Italy and the mountainous regions of the Alps. Notably, Italy and the Alps are the regions within our domain that exhibit the highest biases and lowest correlations with respect to wind direction and speed (Section 4.1), which could explain the poorer temporal correlation for O_3 in these areas.

Looking at Tables 5 and 6, we see some differences in the statistical performance of the MOZART simulation when compared to the EMEP vs. the AirBase observational datasets. Considering the EMEP observations over the whole domain (Table 6), MOZART slightly overpredicts O_3 in summer, with a summertime mean bias of 4 $\mu g\,m^{-3}$, whereas the summertime mean bias when compared the AirBase network is 10 $\mu g\,m^{-3}$ (Table 5). In winter and spring, the bias (MB, NMB, and MFB) in MOZART-predicted O_3 is more negative when compared to EMEP observations than to AirBase observations. In fall, the sign of the domain-average bias changes if considering the model performance against EMEP vs. AirBase observations. These differences likely reflect differences in the character of the two observational networks. First, we expect that the Airbase rural background sites considered here may be, on average, more influenced by local pollution sources than the EMEP sites, which are selected to be representative of more remote regional background. Secondly, the geographical coverage of AirBase vs. EMEP sites for O_3 is slightly different (Supplementary Material). In particular, coverage of the U.K. and the Nordic countries is almost exclusively via the EMEP network, potentially giving the EMEP observations a northern bias in comparison to the AirBase-only sites. Both features of the measurement networks could explain the lower values of the domain-wide average O_3 observed at the EMEP vs. the AirBase stations.

In addition to evaluating the model's ability to simulate hourly O_3 concentrations, we also consider MDA8 and SOMO35, two metrics designed to evaluate the impact of ozone on health. The distribution of seasonal average values of MDA8 is shown in Figure 6 for the MOZART simulation. The European Union's Air Quality Directive states that, as a long-term objective, MDA8 should not exceed the threshhold value of 120 $\mu g\,m^{-3}$; as a target value this long-term objective should not be exceeded on more than 25 days per year, averaged over 3 years. Figure 6 shows that, at some stations in the Alps and in southern Italy during summer, the average value of MDA8 exceeds 120 $\mu g\,m^{-3}$. As seen in Figure 7, the number of days when MDA8 exceeds the 120 $\mu g\,m^{-3}$ is greater than 25 in spring alone for much of southern Europe, which is also captured well by the MOZART simulation. MOZART tends to overpredict MDA8 and the days in exceedance of the target value in summer and fall, consistent with the overestimation of hourly average O_3 during this season. Since the metric MDA8 is, in effect, a measure of daytime ozone, it is always higher than the straight average of hourly concentrations. As a consequence, MOZART shows greater bias in MDA8 than in average O_3 in seasons where average O_3 is already overpredicted (Tables 5 and 6). In general, regional and

Geosci. Model Dev. Discuss., doi:10.5194/gmd-2016-131, 2016
Manuscript under review for journal Geosci. Model Dev.
Published: 7 June 2016

Geoscientific Model Development Discussions
Open Access
EGU

seasonal patterns for MDA8 simulated by MOZART are similar to those for simulated average O_3. SOMO35, an indicator for cumulative annual exposure, is shown in Figure 8 for the year 2007. MOZART is able to reproduce the north-south gradient of SOMO35 seen in the observations quite well, while overpredicting the magnitude of SOMO35 by 2 $\mathrm{mg\,m^{-3}\cdot days}$ (Table 7).

WRF-Chem simulations using the RADM2 chemical mechanism show a spatial and seasonal distribution of surface O_3 over Europe (Figures 9 and 10) that is qualitatively similar to that for MOZART. The correlation coefficients for the MOZART and RADM2 simulations are also similar in both magnitude in distribution. However, it is striking to note that the surface O_3 concentrations predicted by two different chemical mechanisms are quite different, with RADM2 predicting average surface O_3 values that are approximately 20 $\mu\mathrm{g\,m^{-3}}$ lower than those predicted by MOZART in spring and summer (c.f. Figures 4 and 9, Tables 5 and 8, and Tables 6 and 9). In contrast to MOZART, RADM2 underpredicts O_3 throughout most of Europe in all seasons. An exception to this is in southern Europe in winter, where RADM2, like MOZART, shows some overprediction of O_3 concentrations in southern Europe, particularly near the Mediterranean. RADM2 also overpredicts O_3 near the Mediterranean in fall (a season where MOZART overpredicts O_3 Europe-wide). The general underprediction of O_3 concentrations in RADM2 means that the health metrics MDA8 and SOMO35 are also underpredicted (Tables 7- 8 and Figure 8). Overall, absolute biases (i.e., the absolute value of MB, NMB, and MFB) are smaller for MOZART than for RADM2, indicating that MOZART is more successful overall in reproducing European ground-level O_3.

Model biases for O_3 in both the MOZART and RADM2 simulations are in line with biases found in other regional modeling studies for Europe. For instance, values for the NMB in European summertime O_3 ranged from less than -20% to greater than +20% depending on the ensemble member in AQMEII (Solazzo et al., 2012b; Im et al., 2015), compared to values of -18% and +14% for the RADM2 and MOZART simulations, respectively, in the present study. Zhang et al. (2013b) found domain-wide values for NMB for O_3 ranging from +4.2% to +19.1% for the month of July 2001, depending on their model configuration. Tuccella et al. (2012) report a domain-average mean bias in O_3 of -1.4 $\mu\mathrm{g\,m^{-3}}$ averaged over the whole year. Although the work of Tuccella et al. (2012) uses the RADM2 chemical mechanism and simulates the year 2007, similar to the RADM2 simulation in the present study, there are several differences in model configuruation that could explain the observed differences in predicted O_3, including the use of time-invariant chemical boundary conditions, the use of the QSSA rather than the Rosenbrock chemical solver (which has been shown to make a difference (see Forkel et al., 2015)), and the use of an alternate emissions inventory (from EMEP).

The temporal correlation with hourly measurements for O_3 in this study are also in line with other regional modeling studies of O_3 for Europe. Simulations with both chemical mechanisms lead to reasonable correlations between the model-predicted and observed O_3 concentrations over the entire domain, with r values generally in the range of 0.6-0.8 (Figures 5 and 10, Tables 5 and 8).

Geosci. Model Dev. Discuss., doi:10.5194/gmd-2016-131, 2016
Manuscript under review for journal Geosci. Model Dev.
Published: 7 June 2016

Geoscientific Model Development Discussions
Open Access
EGU

This is consistent with the hourly correlation coefficient for O_3 of 0.62 reported by Tuccella et al. (2012), where their r value represents an average over the entire year of 2007. Zhang et al. (2013b) also report correlation coefficients of 0.6-0.7 for hourly O_3 over the European domain (horizontal resolution 0.5°) using the CB05 gas-phase chemical mechanism in WRF-Chem.

In addition to evaluating the performance of the MOZART and RADM2 simulations on their ability to reproduce ground-level ozone concentrations, we compare the observed sensitivity of modeled O_3 to the choice of chemical mechanism to other studies that have investigated the uncertainty in 3-D model predictions associated with the choice of chemical mechanism. Knote et al. (2015) used box model simulations based on AQMEII phase 2, and concluded that the uncertainty in predicted O_3 in a 3-D model solely due to the choice of gas phase chemical mechanism should be of the order of 5%, or 4 ppbv (8 $\mu g\,m^{-3}$). This is quite a bit smaller than the sensitivity to chemical mechanism found in this study, where we see differences in summertime average O_3 of 20 $\mu g\,m^{-3}$, corresponding to a relative difference of approximately 40%. Coates et al. (2016) have shown that accounting for stagnant conditions in a box model increased the variability in predicted O_3 with temperature in a way that better reproduced the variability seen in observational datasets and 3-D model simulations; adding representation of stagnant conditions (which were not represented in Knote et al. (2015)) to the box model also increased the sensitivity of predicted O_3 to the chemical mechanism. This result suggests that day-to-day variability in meteorological conditions and transport can enhance the sensitivity of O_3 to chemical mechanism compared to what is seen in box models.

Another interesting basis for comparison is the study of Mallet and Sportisse (2006), who investigate uncertainty in the CTM Polyphemus due to various physical parameterizations, including chemical mechanism (comparing RACM and RADM2), using an ensemble approach. They estimated an overall uncertainty in O_3 concentrations of 17% based on choices for physical parameterizations in general, but identifed the choice of chemical mechanism along with the turbulent closure parameterization as the two most important drivers of this uncertainty. Simulations using the RACM vs. RADM2 mechanisms yielded differences in average O_3 concentrations of 7-13 $\mu g\,m^{-3}$, depending on the other parameterizations used. It is clear that the sensitivity of O_3 to the use of the MOZART vs. RADM2 chemical mechanism in this study is large compared to other studies of mechanism comparisons in 3-D models (see also Luecken et al., 2008; Kim et al., 2010)), though even larger absolute differences in hourly O_3 concentrations (up to 40 ppb, or 80 $\mu g\,m^{-3}$) have been found in studies of episodic ozone (Faraji et al., 2008; Yarwood et al., 2003). It is possible that MOZART and RADM2 as implemented in this study are examples of chemical mechanisms that are extremely different from one another on a spectrum of other commonly-used mechanisms; the differences between the two mechanisms will be further explored in Section 4.3.

Geosci. Model Dev. Discuss., doi:10.5194/gmd-2016-131, 2016
Manuscript under review for journal Geosci. Model Dev.
Published: 7 June 2016

Geoscientific Model Development Discussions
Open Access
EGU

4.2.2 Nitrogen oxides

Seasonal average surface-level NO_x for the MOZART simulation are shown in Figure 11. Several hotspots in the spatial distribution of NO_x mixing ratios are apparent, as expected based on the intensity of emissions in these areas. NO_x hotspots with concentrations of more than 30 $\mu g\,m^{-3}$ are visible over parts of France, Belgium, Germany and Russia. Similar high concentrations are also seen over the marine regions close to Barcelona, Monaco, and southern France. As shown in Table 5, the MOZART simulation slightly underpredicts domain-average NO_x concentrations for all seasons when comparing to AirBase observations. In Figures 12 and 13 we examine the spatial distribution of NO_x broken down into its components, NO_2 and NO, together with the spatial distribution of MB and r. The MOZART simulation overestimates NO_2 in the U.K., northern France, Belgium, and central Germany, all of which are regions known for having high NO_x emissions and concentrations. However this does not hold true for the Netherlands, a neighboring region with high emissions where MOZART tends to underpredict rather than overpredict NO_2 concentrations. NO, on the other hand, is significantly underpredicted compared to surface measurements throughout the domain. This may be partially due to the relatively coarse horizontal resolution of the model, in which fresh NO emissions are immediately diluted over a large area, and could also be a consequence of model deficiencies in representing NO_x chemical cycles. Artifacts related to reporting of low NO concentrations approaching measurement detection limits could also play a role (observed time series for NO typically show a baseline of 1-2 $\mu g\,m^{-3}$, whereas modeled concentrations reach a baseline of zero).

Domain average temporal correlation coefficients (r) against hourly measurements of NO_x, NO_2, and NO (Tables 5 and 6) range from approximately 0.2 to 0.5, which is lower than correlations for O_3 but consistent with other studies, dicussed further below. In all seasons, the domain-averaged temporal correlation coeffiecient is higher when compared to EMEP vs. AirBase observations. This is attributed to lesser local influences and therefore better regional representativeness of the EMEP stations. No exceptional patterns are seen in the spatial distribution of r for NO_2 or NO, although correlation appears slightly better in the northern part of the domain. The MOZART simulation shows the highest domain-average correlation coefficients (r) for NO_x, NO_2, and NO in winter and fall, and the lowest domain-average r values in summer.

NO_x predicted by the RADM2 simulation shows fairly similar behavior to NO_x predicted by the MOZART simulation (cf. Figures 12 and 14 and additional figures in the Supplementary Material). In general, simulated NO_x concentrations are slightly higher for MOZART than for RADM2. Domain-wide average NO_x concentrations predicted by MOZART are approximately 2 $\mu g\,m^{-3}$ higher than for RADM2 in all seasons except winter, where the difference is approximately 3 $\mu g\,m^{-3}$ (cf. Tables 5 and 8). The spatial distribution of MB for NO_2 for the RADM2 simulation generally shows the same patterns as observed for the MOZART simulation, namely a slight overestimation in the U.K., northern France, Belgium, and central Germany. Temporal correlation is also found to

Geosci. Model Dev. Discuss., doi:10.5194/gmd-2016-131, 2016
Manuscript under review for journal Geosci. Model Dev.
Published: 7 June 2016

show similar behavior to the MOZART simulation. An exception to the similarity observed between the mechanisms for NO_x can be seen over central Germany in winter, where MB values for NO_2 are 6-10 $\mu g\,m^{-3}$ for MOZART, but in the range of 0-6 $\mu g\,m^{-3}$ for RADM2 (ref supplementary material for RADM2 plot). Differences in NO_x concentrations predicted by the MOZART vs. RADM2 simulations are generally less than 20%, consistent with Knote et al. (2015), who conclude that uncertainty due to choice in chemical mechanism leads to an uncertainty of up to 25% in 3-D model simulations.

Performance of the present simulations with respect to NO_2 can also be compared to previous published studies (note that none of the above-cited studies perform a validation for NO or NO_x). Zhang et al. (2013b) reports NMB values of approximately -15% for NO_2 for WRF-Chem simulations against hourly AirBase measurements for July 2001, in line with values of -12% and -19% for the MOZART and RADM2 simulations in this study, respectively. Tuccella et al. (2012) report a MB for NO_2 of -0.9 $\mu g\,m^{-3}$ averaged over the whole year; for comparison the RADM2 simulation in this study shows a MB in the range of -2.5 to -1 $\mu g\,m^{-3}$ for fall, spring and summer, but a MB of +0.67 $\mu g\,m^{-3}$ in summer. Evaluation of NO_2 was not treated in detail in the AQMEII studies, but Im et al. (2015) report that the models for the European domain underestimate NO_2 by 9% to 45%.

4.3 Characterization of MOZART vs. RADM2 differences

In this section, we explore the differences in surface O_3 between the MOZART and RADM2 simulations by examining net O_3, NO_2, and NO production rates as well as the NO_x- and VOC-sensitivity of the two mechanisms. We further conducted sensitivity simulations to investigate the relative contributions of different sources to the observed differences in surface O_3 predicted by MOZART and RADM2. The month of July was chosen for the sensitivity simulations since O_3 concentrations over Europe are highest during summer, and thus summer is most the most important season when considering air quality exceedances and health impacts of O_3. Additionally, MOZART and RADM2 show the largest differences in predicted O_3 during this season (see Tables 5 and 8).

To gain insight into model behavior for O_3, we added terms to the model output representing hourly accumulated tendencies, i.e., the change in concentration of a species due to photochemistry only, for July simulations using MOZART and RADM2. The hourly net photochemical production rate was calculated as the difference in the accumulated tendency from one timestep to another. Figure 15 shows the average of the midday (11:00-14:00 CEST, or 9:00-12:00 UTC) photochemical production rate of O_3 and NO_x components for both the MOZART and RADM2 simulations. (Note that the net photochemical production rate is shown here in $ppb\,hr^{-1}$ for more intuitive comparison of production and loss of the different species on a mole basis; $\mu g\,m^{-3}$ was used in Section 4.2 because this is the unit in which limit and target values in the EU Air Quality Directive are expressed.)

Overall, the spatial variability as well as the magnitudes of net O_3 production rates are found to be similar for MOZART-4 and RADM2 chemistry (Figure 15). For both mechanisms, the greatest

Geosci. Model Dev. Discuss., doi:10.5194/gmd-2016-131, 2016
Manuscript under review for journal Geosci. Model Dev.
Published: 7 June 2016

Geoscientific Model Development Discussions
Open Access
EGU

midday net O_3 production rates are found in southern Europe, particularly over the Mediterranean and Atlantic coasts. The difference in net O_3 production rate between the two mechanisms is also shown in Figure 15. MOZART exhibits greater net O_3 photochemical production rates than RADM2 for most of Europe, with the exception of the southeast corner of the domain (Greece, Turkey, and the nearby Mediterranean), where net O_3 production rates are greater for RADM2. The difference in net O_3 production rate (MOZART-RADM2) shows a large maximum over central Europe, centering over Germany and extending west and east into France and Poland. Over Germany, net O_3 production in MOZART is seen to be higher than in RADM2 by 1.8 $\mathrm{ppb\,hr^{-1}}$ or more.

As expected, regions of high NO_2 production in both MOZART and RADM2 simulations are seen over the high NO_x-emission regions including Benelux, southern England, western Germany, the Po Valley, and major cities including Paris and Moscow. The difference in net NO_2 production rate between the two mechanisms is also highest where the absolute NO_2 production rates are highest; in these areas the net NO_2 production rate is lower for MOZART than for RADM2 by greater than 0.25 $\mathrm{ppb\,hr^{-1}}$. Furthermore, areas where the two mechanisms show the greatest differences in net NO_2 production rate tend to be the areas where the net O_3 production rate is most different between the two mechanisms, including the large maximum over the Netherlands and northwest Germany.

To further investigate the differences between ozone chemistry in MOZART vs. RADM2, we performed two additional sensitivity studies with each mechanism: one in which all anthropogenic NO_x emissions were increased by 30%, and one in which all anthropogenic VOC emissions are increased by 30%. We then examined the change in O_3 concentrations due to these emission perturbations to diagnose whether the chemical mechanisms are operating in a NO_x-sensitive or a VOC-sensitive regime. Results are shown in Figure 16. For the sensitivities where NO_x emissions were increased by 30%, MOZART and RADM2 simulations show very similar behavior. Most of the domain is NO_x sensitive, with increased NO_x emissions resulting in increased modeled O_3. Notably, the U.K., Benelux, northern France and Paris, and northwest Germany show NO_x titration behavior, in which increased NO_x emissions lead to decreased O_3 concentrations. NO_x titration behavior is also seen around the area of the Mediterranean between Monaco, Genoa and Corsica. Magnitudes of the observed change in O_3 are quite similar for both mechanisms, although RADM2 shows slightly stronger NO_x titration in the area centered around Benelux, and stronger NO_x sensitivity over Scandinavia and northwest Russia.

In contrast to the similar behavior seen for NO_x sensitivity, the VOC sensitivity exhibited by the mechanisms is quite different (Figure 16, lower panel). For both MOZART and RADM2, the effect of increased anthropogenic VOC emissions on O_3 is smaller than the effect of increased NO_x emissions. The MOZART simulation shows very little impact of increased VOC emissions on O_3, with differences in average O_3 concentration generally confined to $\pm$ 2% of the base simulation. In contrast, increasing VOC emissions in the RADM2 simulations leads to increased O_3 concentrations

Geosci. Model Dev. Discuss., doi:10.5194/gmd-2016-131, 2016
Manuscript under review for journal Geosci. Model Dev.
Published: 7 June 2016

558 throughout nearly the entire domain. However, the increase in O_3 concentration is modest, generally
559 limited to increases of 2-4% over the base simulation.

560 Taken as a whole, Figure 16 shows that MOZART behaves in a classically NO_x-sensitive manner
561 for most of domain, with O_3 responding to changes in NO_x but showing little response to changes in
562 anthropogenic VOC. NO_x titration behavior is also observed, particularly around the area of U.K.,
563 Benelux, and northern France and Germany. RADM2, on the other hand, exhibits more of a mixed
564 NO_x- VOC-sensitivity for much of the domain. The NO_x sensitivity seen in RADM2 is very similar
565 to that seen in MOZART, but the response of RADM2 to changes in VOC is much stronger (by about
566 a factor of two) than observed in MOZART. With the exception of some small areas in the North
567 and Baltic Sea south of Norway and Sweden, RADM2 predicts O_3 increases with VOC increases
568 throughout the entire domain.

569 In addition to characterizing mechanism behavior with respect to net photochemical O_3 produc-
570 tion and NO_x- and VOC-sensitivity, we evaluate the contribution of other sources that could ex-
571 plain the large differences in predicted O_3 between the MOZART and RADM2 simulations. First,
572 MOZART uses different rate constants for several inorganic gas phase chemical reactions. To test the
573 effect of these differences all RADM2 inorganic reaction rates were changed so that they matched
574 those used in MOZART simulations in the cases where the reactions are the same in both mecha-
575 nisms (Supplementary Material). The differences in inorganic rate constants between the two mech-
576 anisms explain a significant difference in predicted O_3 concentrations: when RADM2 is run with
577 inorganic rate constants from MOZART, the resulting domain-mean O_3 is higher by more than
578 8 $\mu g\,m^{-3}$ for the month of July, approximately 40% of the difference in predicted O_3.

579 Besides the gas-phase chemistry itself, there are some differences in the implementation of MOZART-
580 4 vs. RADM2 in WRF-Chem that could also contribute to the observed differences in modeled O_3:
581 in particular, in the treatment of dry deposition and photolysis (described in the Supplementary Ma-
582 terial). To test the effect of differences in treatment of dry deposition, we conducted an additional
583 sensitivity in which we modified the RADM2 simulation to treat dry deposition in the same way as
584 it is treated in MOZART. However, this led to only a small difference in average ozone (an increase
585 of 1 $\mu g\,m^{-3}$), indicating that modeled surface O_3 concentrations are relatively insensitive to these
586 differences in the treatment of dry deposition, at least in the summer. In a sensitivity test where we
587 modified the model code so that the MOZART simulation ran with the same photolysis scheme as
588 used in our RADM2 simulation (i.e., with the Madronich TUV scheme and without reading in cli-
589 matological O_3 and O_2 columns), we found that average O_3 for July decreases by 3 $\mu g\,m^{-3}$. This
590 indicates that modeled O_3 is also somewhat sensitive to differences in the treatment of photolysis
591 in MOZART and RADM2. However, taken together, our sensitivity simulations suggest that the dif-
592 ferences in the inorganic reaction rate coefficients are more impoprtant than the differing treatments
593 of dry deposition and photolysis in explaining the differences in predicted O_3 between the RADM2
594 and MOZART simulations.

Geosci. Model Dev. Discuss., doi:10.5194/gmd-2016-131, 2016
Manuscript under review for journal Geosci. Model Dev.
Published: 7 June 2016

Geoscientific Model Development Discussions
Open Access
EGU

5 Summary and Conclusions

In this paper, we present a detailed description of a WRF-Chem setup over the European domain and provide an evaluation of the simulated meteorological and chemical fields with an emphasis on model's ability to reproduce the spatial and temporal distribution of ground-level O_3 and NO_x. Within WRF-Chem we compare the performance of two different chemical mechanisms: MOZART-4, for which we present the first model evaluation for a European domain, and RADM2. Overall, we found that our WRF-Chem setup reproduced the spatial and seasonal variations in the meteorological parameters over Europe, with biases and correlations consistent with previous studies. Simulations using the MOZART-4 as well as RADM2 chemical mechanisms were found to reproduce the spatial and temporal distributions in ground-level O_3 over Europe, based on observations from the EMEP and Airbase networks. However, we find significant differences in O_3 concentrations predicted by the two chemical mechanisms, with RADM2 predicting as much as 20 $\mu g\,m^{-3}$ less O_3 than MOZART during the spring and summer seasons. In general, MOZART-4 chemistry overpredicts O_3 concentrations for most of Europe in the summer and fall, whereas RADM2 leads to an underestimation of O_3 over the European domain in all seasons. Taken as a whole, use of MOZART-4 chemistry performs better, leading to lower absolute model biases in O_3. This is the case when considering hourly O_3 concentrations as well as metrics relevant for human health, such as MDA8 and SOMO35. Despite the large differences in predicted O_3, the two mechanisms show relatively similar behavior for NO_x, with both MOZART and RADM2 simulations resulting in a slight underestimation of NO_x compared to surface observations.

The net midday photochemical production rate of O_3 in summer is found to be higher for MOZART than for RADM2 for most of the domain, with the largest differences between the mechanisms seen over Germany, where the net O_3 photochemical production for MOZART is higher than for RADM2 by greater than 1.8 $ppb\,hr^{-1}$ (3.6 $\mu g\,m^{-3}\,hr^{-1}$). However, we have shown that RADM2 is approximately twice as sensitive to increases in anthropogenic VOC emissions as MOZART, suggesting that, under local VOC-limited conditions not seen at the regional scale of our simulations, RADM2 is likely to produce O_3 at a greater rate than MOZART. Despite the differences in sensitivity to changes in VOC emissions exhibited by the two mechanisms, sensitivity to changes in NO_x emissions in MOZART and RADM2 are found to be similar.

Our results indicate that modeled surface O_3 over Europe is sensitive the choice of gas phase chemical mechanism, with observed differences in O_3 between mechanisms that are larger than those seen in many past studies. Although the most fundamental differences between MOZART-4 and RADM2 (and other chemical mechanisms used in regional modeling) is the representation of VOC oxidation chemistry, we find that approximately 40% of the difference seen in predicted O_3 seen in this study can be explained by differences in inorganic reaction rate constants employed by MOZART-4 and RADM2. Further investigation of chemical mechanism behavior within 3-D models would be helpful to constrain uncertainties in regional air quality modeling.

Geosci. Model Dev. Discuss., doi:10.5194/gmd-2016-131, 2016
Manuscript under review for journal Geosci. Model Dev.
Published: 7 June 2016

Geoscientific Model Development Discussions
Open Access
EGU

6 Code availability

The WRF-Chem model is an open-source, publicly available software. The code is being continually improved, with new releases approximately twice per year. WRF-Chem code can be downloaded at (http://www2.mmm.ucar.edu/wrf/users/download/get_source.html). The corresponding author will provide the bug fixes to version 3.5.1 used in this study, described in Section 2.3, upon request.

Appendix A: Abbreviations and Acronyms

DJF: December-January-February (winter)
EDGAR: Emission Database for Global Atmospheric Research
EEA: European Environmental Agency
EOS: Earth Observing System
GEOS5: Goddard Earth Observing System Model, Version 5
GOCART: Goddard Chemistry Aerosol Radiation and Transport
HTAP: Hemispheric Transport of Air Pollution
JJA: June-July-August (summer)
MADE: Modal Aerosol Dynamics Model for Europe
MAM: March-April-May (spring)
MERRA: Modern Era-Retrospective Analysis for Research and Applications
NCEP: National Centers for Environmental Prediction
NCAR: National Center for Atmospheric Research
SON: September-October-November (fall)
SORGAM: Secondary Organic Aerosol Model
WRF-Chem: Weather Research and Forecasting with Chemistry

Appendix B: Definitions of statistical quantities

The statistical quantities used for model evaluation are defined below. Let Obs_i^j and Mod_i^j be the observed and modeled quantities at time i and station j, respectively. N_{obs}^j represents the number of temporal data points evaluated at station j, and N_{obs} represents the total number of data points (each representing a time i and a station j) evaluated in the domain.

The Mean Bias (MB) at a specific station (e.g., Figure 5) is calculated as

$$MB^j = \frac{1}{N_{obs}^j} \sum_{i=1}^{N_{obs}^j} Mod_i^j - Obs_i^j$$

and the domain-wide Mean Bias (e.g., Table 5) as

$$MB = \frac{1}{N_{obs}} \sum_{i,j=1}^{N_{obs}} Mod_i^j - Obs_i^j$$

Geosci. Model Dev. Discuss., doi:10.5194/gmd-2016-131, 2016
Manuscript under review for journal Geosci. Model Dev.
Published: 7 June 2016

Geoscientific Model Development Discussions
Open Access
EGU

Domain-wide values for Normalized Mean Bias (NMB) and Mean Fractional Bias (MFB) are calculated analogously.

$$NMB = \frac{\sum_{i=1}^{N_{obs}} Mod_i^j - Obs_i^j}{\sum_{i=1}^{N_{obs}} Obs_i^j}$$

$$MFB = \frac{1}{N_{obs}} \sum_{i,j=1}^{N_{obs}} \frac{Mod_i^j - Obs_i^j}{\frac{Mod_i^j + Obs_i^j}{2}}$$

Temporal correlation between model results and observation is evaluated using the Pearson correlation coefficient (r). The value of r is calculated at each station using

$$r^j = \frac{\sum_{i=1}^{N_{obs}^j} \left(Mod_i^j - \overline{Mod^j}\right)\left(Obs_i^j - \overline{Obs^j}\right)}{\sigma_{mod} \times \sigma_{obs}}$$

Here, the numerator represents the covariance between the model and observations, $\overline{Mod^j}$ and $\overline{Obs^j}$ represent the mean of the model and observations, respectively, and σ is the standard deviation. The domain-wide correlation coefficients (e.g., Table 5) is then calculated as

$$r = \frac{1}{N_j} \sum_{j}^{N_j} r^j$$

where N_j is the total number of stations.

Acknowledgements. The authors would like to thank Renate Forkel for valuable discussions regarding the setup of our WRF-Chem simulation. The authors also thank Jane Coates for sharing her technique for VOC speciation and valuable discussions regarding chemical mechanisms. We thank TNO for access to the TNO-MACC II emissions inventory, and Hugo Denier van der Gon for helpful discussions regarding emissions. The HTAP v2.2 anthropogenic emissions were obtained from http://edgar.jrc.ec.europa.eu/htap_v2/index.php. The authors thank Christophe Knote and Anna Katinka Petersen for sharing bug fixes for the WRF-Chem MOZART code. WRF-Chem tools for preprocessing boundary conditions as well as biogenic, fire, and anthropogenic emissions were provided by NCAR (http://www.acom.ucar.edu/wrf-chem/download.shtml). Initial and boundary conditions for meteorological fields were obtained from ECMWF, http://www.ecmwf.int/en/research/climate-reanalysis/era-interim. Initial and boundary conditions for chemical fields were from MOZART-4/GEOS5, provided by NCAR at http://www.acd.ucar.edu/wrf-chem/mozart.shtml. Corine land cover data was obtained from http://www.eea.europa.eu/data-and-maps/data/corine-land-cover-2006-raster-2. We acknowledge the UK Met Office for providing the Global Weather Observation dataset via the British Atmospheric Data Centre. We acknowledge EMEP and the Norwegian Institute for Air Research (NILU) for providing the EMEP chemical observation data via the EBAS database (ebas.nilu.no). AirBase is the public air quality database of the EEA; data were obtained at http://www.eea.europa.eu/data-and-maps/data/airbase-the-european-air-quality-database-7. The WRF-Chem simulations have been performed on the supercomputer HYDRA (http://www.rzg.mpg.de/).

Geosci. Model Dev. Discuss., doi:10.5194/gmd-2016-131, 2016
Manuscript under review for journal Geosci. Model Dev.
Published: 7 June 2016

692 **References**

693 Ackermann, I. J., Hass, H., Memmesheimer, M., Ebel, A., Binkowski, F. S., and Shankar, U.: Modal aerosol
694 dynamics model for Europe: development and first applications, Atmospheric Environment, 32, 2981 –
695 2999, doi:http://dx.doi.org/10.1016/S1352-2310(98)00006-5, http://www.sciencedirect.com/science/article/
696 pii/S1352231098000065, 1998a.
697 Ackermann, I. J., Hass, H., Memmesheimer, M., Ebel, A., Binkowski, F. S., and Shankar, U.: Modal aerosol
698 dynamics model for Europe: development and first applications, Atmospheric Environment, 32, 2981 –
699 2999, doi:http://dx.doi.org/10.1016/S1352-2310(98)00006-5, http://www.sciencedirect.com/science/article/
700 pii/S1352231098000065, 1998b.
701 Baklanov, A., Schlünzen, K., Suppan, P., Baldasano, J., Brunner, D., Aksoyoglu, S., Carmichael, G., Douros, J.,
702 Flemming, J., Forkel, R., Galmarini, S., Gauss, M., Grell, G., Hirtl, M., Joffre, S., Jorba, O., Kaas, E., Kaasik,
703 M., Kallos, G., Kong, X., Korsholm, U., Kurganskiy, A., Kushta, J., Lohmann, U., Mahura, A., Manders-
704 Groot, A., Maurizi, A., Moussiopoulos, N., Rao, S. T., Savage, N., Seigneur, C., Sokhi, R. S., Solazzo,
705 E., Solomos, S., Sørensen, B., Tsegas, G., Vignati, E., Vogel, B., and Zhang, Y.: Online coupled regional
706 meteorology chemistry models in Europe: current status and prospects, Atmospheric Chemistry and Physics,
707 14, 317–398, doi:10.5194/acp-14-317-2014, http://www.atmos-chem-phys.net/14/317/2014/, 2014.
708 Beljaars, A. C. M.: The parametrization of surface fluxes in large-scale models under free convection, Quarterly
709 Journal of the Royal Meteorological Society, 121, 255–270, doi:10.1002/qj.49712152203, http://dx.doi.org/
710 10.1002/qj.49712152203, 1995.
711 Bieser, J., Aulinger, A., Matthias, V., Quante, M., and Denier van der Gon, H.: Vertical emission
712 profiles for Europe based on plume rise calculations, Environmental Pollution, 159, 2935–2946,
713 doi:10.1016/j.envpol.2011.04.030, 2011.
714 Binkowski, F. S. and Shankar, U.: The Regional Particulate Matter Model: 1. Model description and preliminary
715 results, Journal of Geophysical Research: Atmospheres, 100, 26 191–26 209, doi:10.1029/95JD02093, http:
716 //dx.doi.org/10.1029/95JD02093, 1995.
717 Carter, W. P.: A detailed mechanism for the gas-phase atmospheric reactions of organic compounds, At-
718 mospheric Environment. Part A. General Topics, 24, 481 – 518, doi:http://dx.doi.org/10.1016/0960-
719 1686(90)90005-8, http://www.sciencedirect.com/science/article/pii/0960168690900058, 1990.
720 Chen, F. and Dudhia, J.: Coupling and advanced land surface-hydrology model with the Penn State-NCAR
721 MM5 modeling system, Part I: Model implementation and sensitivity, Mon. Weather Rev., 129, 569–585,
722 2001.
723 Chou, M.-D. and Suarez, M. J.: An efficient thermal infrared radiation parametrization for use in general circu-
724 lation models, NASA Tech. Memo., 104606, 85 pp., 1994.
725 Coates, J. and Butler, T. M.: A comparison of chemical mechanisms using tagged ozone production potential
726 (TOPP) analysis, Atmospheric Chemistry and Physics, 15, 8795–8808, doi:10.5194/acp-15-8795-2015, http:
727 //www.atmos-chem-phys.net/15/8795/2015/, 2015.
728 Coates, J., Mar, K., Ojha, N., and Butler, T.: The Influence of Temperature on Ozone Production under vary-
729 ing NOx Conditions – a modelling study, Atmospheric Chemistry and Physics Discussions, 2016, 1–18,
730 doi:10.5194/acp-2016-260, http://www.atmos-chem-phys-discuss.net/acp-2016-260/, 2016.

Geosci. Model Dev. Discuss., doi:10.5194/gmd-2016-131, 2016
Manuscript under review for journal Geosci. Model Dev.
Published: 7 June 2016

731 Damian, V., Sandu, A., Damian, M., Potra, F., and Carmichael, G. R.: The kinetic preprocessor KPP-a
732 software environment for solving chemical kinetics, Computers & Chemical Engineering, 26, 1567 –
733 1579, doi:http://dx.doi.org/10.1016/S0098-1354(02)00128-X, http://www.sciencedirect.com/science/article/
734 pii/S009813540200128X, 2002.
735 Denier van der Gon, H., Hendriks, C., Kuenen, J., Segers, A., and Visschedijk, A.: Description of current
736 temporal emission patterns and sensitivity of predicted AQ for temporal emission patterns, TNO report, EU
737 FP7 MACC deliverable report D_D-EMIS_1.3, 2011.
738 EEA: Corine Land Cover 2006 raster data, Copenhagen, Denmark, doi:accessed June 2015, http://www.eea.
739 europa.eu/data-and-maps/data/corine-land-cover-2006-raster-2, 2012.
740 EEA: Air quality in Europe - 2014 report, Tech. Rep. 5/2014, European Environmental Agency,
741 doi:10.2800/22847, 2014.
742 Emmons, L. K., Walters, S., Hess, P. G., Lamarque, J.-F., Pfister, G. G., Fillmore, D., Granier, C., Guenther, A.,
743 Kinnison, D., Laepple, T., Orlando, J., Tie, X., Tyndall, G., Wiedinmyer, C., Baughcum, S. L., and Kloster, S.:
744 Description and evaluation of the Model for Ozone and Related chemical Tracers, version 4 (MOZART-4),
745 Geoscientific Model Development, 3, 43–67, doi:10.5194/gmd-3-43-2010, http://www.geosci-model-dev.
746 net/3/43/2010/, 2010.
747 Faraji, M., Kimura, Y., McDonald-Buller, E., and Allen, D.: Comparison of the carbon bond and {SAPRC}
748 photochemical mechanisms under conditions relevant to southeast Texas, Atmospheric Environment, 42,
749 5821 – 5836, doi:http://dx.doi.org/10.1016/j.atmosenv.2007.07.048, http://www.sciencedirect.com/science/
750 article/pii/S1352231007006565, selected Papers from the First International Conference on Atmospheric
751 Chemical Mechanisms, 2008.
752 Forkel, R., Balzarini, A., Baró, R., Bianconi, R., Curci, G., Jiménez-Guerrero, P., Hirtl, M., Hon-
753 zak, L., Lorenz, C., Im, U., Pérez, J. L., Pirovano, G., José, R. S., Tuccella, P., Werhahn, J., and
754 Žabkar, R.: Analysis of the WRF-Chem contributions to {AQMEII} phase2 with respect to aerosol
755 radiative feedbacks on meteorology and pollutant distributions, Atmospheric Environment, 115, 630
756 – 645, doi:http://dx.doi.org/10.1016/j.atmosenv.2014.10.056, http://www.sciencedirect.com/science/article/
757 pii/S135223101400853X, 2015.
758 Geiger, H., Barnes, I., Bejan, I., Benter, T., and Spittler, M.: The tropospheric degradation of isoprene: an
759 updated module for the regional atmospheric chemistry mechanism, Atmospheric Environment, 37, 1503 –
760 1519, doi:http://dx.doi.org/10.1016/S1352-2310(02)01047-6, http://www.sciencedirect.com/science/article/
761 pii/S1352231002010476, 2003.
762 Gery, M. W., Whitten, G. Z., Killus, J. P., and Dodge, M. C.: A photochemical kinetics mechanism for urban
763 and regional scale computer modeling, Journal of Geophysical Research: Atmospheres, 94, 12 925–12 956,
764 doi:10.1029/JD094iD10p12925, http://dx.doi.org/10.1029/JD094iD10p12925, 1989.
765 Grell, G. A. and Dévényi, D.: A generalized approach to parameterizing convection combining ensemble and
766 data assimilation techniques, Geophysical Research Letters, 29, 38–1–38–4, doi:10.1029/2002GL015311,
767 http://dx.doi.org/10.1029/2002GL015311, 2002.
768 Grell, G. A., Knoche, R., Peckham, S. E., and McKeen, S. A.: Online versus offline air quality modeling
769 on cloud-resolving scales, Geophysical Research Letters, 31, n/a–n/a, doi:10.1029/2004GL020175, http:
770 //dx.doi.org/10.1029/2004GL020175, l16117, 2004.

771 Grell, G. A., Peckham, S. E., Schmitz, R., McKeen, S. A., Frost, G., Skamarock, W. C., and
772 Eder, B.: Fully coupled "online" chemistry within the WRF model, Atmospheric Environment, 39,
773 doi:10.1016/j.atmosenv.2005.04.027, http://dx.doi.org/10.1016/j.atmosenv.2005.04.027, 2005.
774 Guenther, A., Karl, T., Harley, P., Wiedinmyer, C., Palmer, P. I., and Geron, C.: Estimates of global terrestrial
775 isoprene emissions using MEGAN (Model of Emissions of Gases and Aerosols from Nature), Atmospheric
776 Chemistry and Physics, 6, 3181–3210, doi:10.5194/acp-6-3181-2006, http://www.atmos-chem-phys.net/6/
777 3181/2006/, 2006.
778 Hong, S.-Y., Noh, Y., and Dudhia, J.: A New Vertical Diffusion Package with an Explicit Treatment of Entrain-
779 ment Processes, Monthly Weather Review, 134, 2318–2341, http://dx.doi.org/10.1175/MWR3199.1, doi:
780 10.1175/MWR3199.1, 2006.
781 Iacono, M. J., Delamere, J. S., Mlawer, E. J., Shephard, M. W., Clough, S. A., and Collins, W. D.: Radiative
782 forcing by long-lived greenhouse gases: Calculations with the AER radiative transfer models, Journal of
783 Geophysical Research: Atmospheres, 113, n/a–n/a, doi:10.1029/2008JD009944, http://dx.doi.org/10.1029/
784 2008JD009944, d13103, 2008.
785 Im, U., Bianconi, R., Solazzo, E., Kioutsioukis, I., Badia, A., Balzarini, A., Baró, R., Bellasio, R., Brun-
786 ner, D., Chemel, C., Curci, G., Flemming, J., Forkel, R., Giordano, L., Jiménez-Guerrero, P., Hirtl, M.,
787 Hodzic, A., Honzak, L., Jorba, O., Knote, C., Kuenen, J. J., Makar, P. A., Manders-Groot, A., Neal, L.,
788 Pérez, J. L., Pirovano, G., Pouliot, G., Jose, R. S., Savage, N., Schroder, W., Sokhi, R. S., Syrakov, D.,
789 Torian, A., Tuccella, P., Werhahn, J., Wolke, R., Yahya, K., Zabkar, R., Zhang, Y., Zhang, J., Hogrefe, C.,
790 and Galmarini, S.: Evaluation of operational on-line-coupled regional air quality models over Europe and
791 North America in the context of {AQMEII} phase 2. Part I: Ozone, Atmospheric Environment, 115, 404
792 – 420, doi:http://dx.doi.org/10.1016/j.atmosenv.2014.09.042, http://www.sciencedirect.com/science/article/
793 pii/S1352231014007353, 2015.
794 Janssens-Maenhout, G., Crippa, M., Guizzardi, D., Dentener, F., Muntean, M., Pouliot, G., Keating, T., Zhang,
795 Q., Kurokawa, J., Wankmüller, R., Denier van der Gon, H., Klimont, Z., Frost, G., Darras, S., and Koffi, B.:
796 HTAP v2: a mosaic of regional and global emission gridmaps for 2008 and 2010 to study hemispheric trans-
797 port of air pollution, Atmospheric Chemistry and Physics Discussions, 15, 12 867–12 909, doi:10.5194/acpd-
798 15-12867-2015, http://www.atmos-chem-phys-discuss.net/15/12867/2015/, 2015.
799 Kim, Y., Sartelet, K., and Seigneur, C.: Comparison of two gas-phase chemical kinetic mechanisms of ozone
800 formation over Europe, Journal of Atmospheric Chemistry, 62, 89–119, doi:10.1007/s10874-009-9142-5,
801 http://dx.doi.org/10.1007/s10874-009-9142-5, 2010.
802 Knote, C., Tuccella, P., Curci, G., Emmons, L., Orlando, J. J., Madronich, S., Baró, R., Jiménez-Guerrero,
803 P., Luecken, D., Hogrefe, C., Forkel, R., Werhahn, J., Hirtl, M., Pérez, J. L., José, R. S., Giordano, L.,
804 Brunner, D., Yahya, K., and Zhang, Y.: Influence of the choice of gas-phase mechanism on predictions of
805 key gaseous pollutants during the {AQMEII} phase-2 intercomparison, Atmospheric Environment, 115, 553
806 – 568, doi:http://dx.doi.org/10.1016/j.atmosenv.2014.11.066, http://www.sciencedirect.com/science/article/
807 pii/S1352231014009388, 2015.
808 Kuenen, J., Visschedijk, J., Jozwicka, M., and Denier van der Gon, H.: TNO-MACC_II emission inven-
809 tory: a multi-year (2003-2009) consistent high-resolution European inventory for air quality modelling,

Atmospheric Chemistry and Physics, 14, 10 963–10 976, doi:10.5194/acp-14-10963-2014, http://www.atmos-chem-phys.net/14/10963/2014/, 2014.

Kuik, F., Churkina, G., Lauer, A., Mar, K., and Butler, T.: Air quality modelling in the Berlin-Brandenburg region: evaluation of a WRF-Chem setup, manuscript in preparation, 2016.

Kusaka, H. and Kimura, F.: Thermal Effects of Urban Canyon Structure on the Nocturnal Heat Island: Numerical Experiment Using a Mesoscale Model Coupled with an Urban Canopy Model, Journal of Applied Meteorology, 43, 1899–1910, http://dx.doi.org/10.1175/JAM2169.1, doi: 10.1175/JAM2169.1, 2004.

Lelieveld, J., Evans, J. S., Fnais, M., Giannadaki, D., and Pozzer, A.: The contribution of outdoor air pollution sources to premature mortality on a global scale, Nature, 525, 367–371, http://dx.doi.org/10.1038/nature15371, letter, 2015.

Lin, Y.-L., Farley, R. D., and Orville, H. D.: Bulk Parameterization of the Snow Field in a Cloud Model, Journal of Climate and Applied Meteorology, 22, 1065–1092, doi:10.1175/1520-0450(1983)022<1065:BPOTSF>2.0.CO;2, http://dx.doi.org/10.1175/1520-0450(1983)022<1065:BPOTSF>2.0.CO;2, 1983.

Liu, P., Tsimpidi, A. P., Hu, Y., Stone, B., Russell, A. G., and Nenes, A.: Differences between downscaling with spectral and grid nudging using WRF, Atmospheric Chemistry and Physics, 12, 3601–3610, doi:10.5194/acp-12-3601-2012, http://www.atmos-chem-phys.net/12/3601/2012/, 2012.

Luecken, D., Phillips, S., Sarwar, G., and Jang, C.: Effects of using the {CB05} vs. {SAPRC99} vs. {CB4} chemical mechanism on model predictions: Ozone and gas-phase photochemical precursor concentrations, Atmospheric Environment, 42, 5805 – 5820, doi:http://dx.doi.org/10.1016/j.atmosenv.2007.08.056, http://www.sciencedirect.com/science/article/pii/S1352231007007728, selected Papers from the First International Conference on Atmospheric Chemical Mechanisms, 2008.

Mallet, V. and Sportisse, B.: Uncertainty in a chemistry-transport model due to physical parameterizations and numerical approximations: An ensemble approach applied to ozone modeling, Journal of Geophysical Research: Atmospheres, 111, n/a–n/a, doi:10.1029/2005JD006149, http://dx.doi.org/10.1029/2005JD006149, d01302, 2006.

Mallet, V., Quélo, D., Sportisse, B., Ahmed de Biasi, M., Debry, E., Korsakissok, I., Wu, L., Roustan, Y., Sartelet, K., Tombette, M., and Foudhil, H.: Technical Note: The air quality modeling system Polyphemus, Atmospheric Chemistry and Physics, 7, 5479–5487, doi:10.5194/acp-7-5479-2007, http://www.atmos-chem-phys.net/7/5479/2007/, 2007.

Miguez-Macho, G., Stenchikov, G., and Robock, A.: Spectral nudging to eliminate the effects of domain position and geometry in regional climate model simulations, Journal of Geophysical Research: Atmospheres, 109, doi:10.1029/2003JD004495, 2004.

Monks, P. S., Archibald, A. T., Colette, A., Cooper, O., Coyle, M., Derwent, R., Fowler, D., Granier, C., Law, K. S., Mills, G. E., Stevenson, D. S., Tarasova, O., Thouret, V., von Schneidemesser, E., Sommariva, R., Wild, O., and Williams, M. L.: Tropospheric ozone and its precursors from the urban to the global scale from air quality to short-lived climate forcer, Atmospheric Chemistry and Physics, 15, 8889–8973, doi:10.5194/acp-15-8889-2015, http://www.atmos-chem-phys.net/15/8889/2015/, 2015.

Pfister, G. G., Walters, S., Emmons, L. K., Edwards, D. P., and Avise, J.: Quantifying the contribution of inflow on surface ozone over California during summer 2008, Journal of Geophysical Research:

Atmospheres, 118, 12,282–12,299, doi:10.1002/2013JD020336, http://dx.doi.org/10.1002/2013JD020336, 2013JD020336, 2013.

Regional Office for Europe, W.: , Tech. rep., World Health Organization, 2008.

Sandu, A. and Sander, R.: Technical note: Simulating chemical systems in Fortran90 and Matlab with the Kinetic PreProcessor KPP-2.1, Atmospheric Chemistry and Physics, 6, 187–195, doi:10.5194/acp-6-187-2006, http://www.atmos-chem-phys.net/6/187/2006/, 2006.

Schaap, M., Roemer, M., Sauter, F., Boersen, G., Timmermans, R., and Builtjes, P.: LOTOS-EUROS: Documentation, TNO report B&O-A, 2005.

Schaap, M., Timmermans, R., Roemer, M., Boersen, G., Builtjes, P., Sauter, F., Velders, G., and Beck, J.: The LOTOS-EUROS model: Description, validation and latest developments, International Journal of Environment and Pollution, 32, 270–290, doi:10.1504/IJEP.2008.017106, http://www.scopus.com/inward/record.url?eid=2-s2.0-39349101242&partnerID=40&md5=af80f203e8a045cbb128dc3b58074135, cited By 0, 2008.

Schell, B., Ackermann, I. J., Hass, H., Binkowski, F. S., and Ebel, A.: Modeling the formation of secondary organic aerosol within a comprehensive air quality model system, Journal of Geophysical Research: Atmospheres, 106, 28 275–28 293, doi:10.1029/2001JD000384, http://dx.doi.org/10.1029/2001JD000384, 2001.

Simpson, D., Benedictow, A., Berge, H., Bergström, R., Emberson, L. D., Fagerli, H., Flechard, C. R., Hayman, G. D., Gauss, M., Jonson, J. E., Jenkin, M. E., Nyíri, A., Richter, C., Semeena, V. S., Tsyro, S., Tuovinen, J.-P., Valdebenito, A., and Wind, P.: The EMEP MSC-W chemical transport model –technical description, Atmospheric Chemistry and Physics, 12, 7825–7865, doi:10.5194/acp-12-7825-2012, http://www.atmos-chem-phys.net/12/7825/2012/, 2012.

Solazzo, E., Bianconi, R., Pirovano, G., Matthias, V., Vautard, R., Moran, M. D., Appel, K. W., Bessagnet, B., Brandt, J., Christensen, J. H., Chemel, C., Coll, I., Ferreira, J., Forkel, R., Francis, X. V., Grell, G., Grossi, P., Hansen, A. B., Miranda, A. I., Nopmongcol, U., Prank, M., Sartelet, K. N., Schaap, M., Silver, J. D., Sokhi, R. S., Vira, J., Werhahn, J., Wolke, R., Yarwood, G., Zhang, J., Rao, S. T., and Galmarini, S.: Operational model evaluation for particulate matter in Europe and North America in the context of {AQMEII}, Atmospheric Environment, 53, 75 – 92, doi:http://dx.doi.org/10.1016/j.atmosenv.2012.02.045, http://www.sciencedirect.com/science/article/pii/S1352231012001604, aQMEII: An International Initiative for the Evaluation of Regional-Scale Air Quality Models - Phase 1, 2012a.

Solazzo, E., Bianconi, R., Vautard, R., Appel, K. W., Moran, M. D., Hogrefe, C., Bessagnet, B., Brandt, J., Christensen, J. H., Chemel, C., Coll, I., van der Gon, H. D., Ferreira, J., Forkel, R., Francis, X. V., Grell, G., Grossi, P., Hansen, A. B., Jeričević, A., Kraljević, L., Miranda, A. I., Nopmongcol, U., Pirovano, G., Prank, M., Riccio, A., Sartelet, K. N., Schaap, M., Silver, J. D., Sokhi, R. S., Vira, J., Werhahn, J., Wolke, R., Yarwood, G., Zhang, J., Rao, S., and Galmarini, S.: Model evaluation and ensemble modelling of surface-level ozone in Europe and North America in the context of {AQMEII}, Atmospheric Environment, 53, 60 – 74, doi:http://dx.doi.org/10.1016/j.atmosenv.2012.01.003, http://www.sciencedirect.com/science/article/pii/S1352231012000064, aQMEII: An International Initiative for the Evaluation of Regional-Scale Air Quality Models - Phase 1, 2012b.

Stauffer, D. R., Seaman, N. L., and Binkowski, F. S.: Use of Four-Dimensional Data Assimilation in a Limited-Area Mesoscale Model Part II: Effects of Data Assimilation within the Planetary Boundary Layer, Mon.

Wea. Rev., 119, 734–754, doi:10.1175/1520-0493(1991)119<0734:UOFDDA>2.0.CO;2, http://dx.doi.org/10.1175/1520-0493(1991)119<0734:UOFDDA>2.0.CO;2, 1991.

Stegehuis, A., Vautard, R., Ciais, P., Teuling, A., Miralles, D., and Wild., M.: An observation-constrained multi-physics RCM ensemble for simulating European mega-heatwaves, Geoscientific Model Development Discussions, 7, 7861–7886, doi:10.5194/gmdd-7-7861-2014, 2014.

Stevenson, D. S., Young, P. J., Naik, V., Lamarque, J.-F., Shindell, D. T., Voulgarakis, A., Skeie, R. B., Dalsoren, S. B., Myhre, G., Berntsen, T. K., Folberth, G. A., Rumbold, S. T., Collins, W. J., MacKenzie, I. A., Doherty, R. M., Zeng, G., van Noije, T. P. C., Strunk, A., Bergmann, D., Cameron-Smith, P., Plummer, D. A., Strode, S. A., Horowitz, L., Lee, Y. H., Szopa, S., Sudo, K., Nagashima, T., Josse, B., Cionni, I., Righi, M., Eyring, V., Conley, A., Bowman, K. W., Wild, O., and Archibald, A.: Tropospheric ozone changes, radiative forcing and attribution to emissions in the Atmospheric Chemistry and Climate Model Intercomparison Project (ACCMIP), Atmospheric Chemistry and Physics, 13, 3063–3085, doi:10.5194/acp-13-3063-2013, http://www.atmos-chem-phys.net/13/3063/2013/, 2013.

Stockwell, W. R., Middleton, P., Chang, J. S., and Tang, X.: The second generation regional acid deposition model chemical mechanism for regional air quality modeling, Journal of Geophysical Research: Atmospheres, 95, 16 343–16 367, doi:10.1029/JD095iD10p16343, http://dx.doi.org/10.1029/JD095iD10p16343, 1990.

Stockwell, W. R., Kirchner, F., Kuhn, M., and Seefeld, S.: A new mechanism for regional atmospheric chemistry modeling, Journal of Geophysical Research: Atmospheres, 102, 25 847–25 879, doi:10.1029/97JD00849, http://dx.doi.org/10.1029/97JD00849, 1997.

Terrenoire, E., Bessagnet, B., Rouïl, L., Tognet, F., Pirovano, G., Létinois, L., Beauchamp, M., Colette, A., Thunis, P., Amann, M., and Menut, L.: High-resolution air quality simulation over Europe with the chemistry transport model CHIMERE, Geoscientific Model Development, 8, 21–42, doi:10.5194/gmd-8-21-2015, http://www.geosci-model-dev.net/8/21/2015/, 2015.

Tørseth, K., Aas, W., Breivik, K., Fjæraa, A. M., Fiebig, M., Hjellbrekke, A. G., Lund Myhre, C., Solberg, S., and Yttri, K. E.: Introduction to the European Monitoring and Evaluation Programme (EMEP) and observed atmospheric composition change during 1972–2009, Atmospheric Chemistry and Physics, 12, 5447–5481, doi:10.5194/acp-12-5447-2012, http://www.atmos-chem-phys.net/12/5447/2012/, 2012.

Tuccella, P., Curci, G., Visconti, G., Bessagnet, B., Menut, L., and Park, R. J.: Modeling of gas and aerosol with WRF/Chem over Europe: Evaluation and sensitivity study, Journal of Geophysical Research: Atmospheres, 117, n/a–n/a, doi:10.1029/2011JD016302, http://dx.doi.org/10.1029/2011JD016302, d03303, 2012.

von Schneidemesser, E., Coates, J., van der Gon, H. D., Visschedijk, A., and Butler, T.: Variation of the {NMVOC} speciation in the solvent sector and the sensitivity of modelled tropospheric ozone, Atmospheric Environment, 135, 59 – 72, doi:http://dx.doi.org/10.1016/j.atmosenv.2016.03.057, http://www.sciencedirect.com/science/article/pii/S1352231016302242, 2016.

Wang, W., Bruyère, C., Duda, M., Dudhia, J., Gill, D., Kavulich, M., Keene, K., Lin, H.-C., Michalakes, J., Rizvi, S., and Zhang, X.: ARW Version 3 Modeling System User's Guide, Chapter 3: WRF Preprocessing System (WPS), pp. 59–60, 2014.

WHO: Health Aspects of Air Pollution with Particulate Matter, Ozone and Nitrogen Dioxide, Bonn, 2003.

929 Wiedinmyer, C., Akagi, S. K., Yokelson, R. J., Emmons, L. K., Al-Saadi, J. A., Orlando, J. J., and Soja, A. J.:
930 The Fire INventory from NCAR (FINN): a high resolution global model to estimate the emissions from
931 open burning, Geoscientific Model Development, 4, 625–641, doi:10.5194/gmd-4-625-2011, http://www.
932 geosci-model-dev.net/4/625/2011/, 2011.
933 Wilson, R. C., Fleming, Z. L., Monks, P. S., Clain, G., Henne, S., Konovalov, I. B., Szopa, S., and Menut, L.:
934 Have primary emission reduction measures reduced ozone across Europe? An analysis of European rural
935 background ozone trends 1996–2005, Atmospheric Chemistry and Physics, 12, 437–454, doi:10.5194/acp-
936 12-437-2012, http://www.atmos-chem-phys.net/12/437/2012/, 2012.
937 Yarwood, G., Stoeckenius, T. E., Heiken, J. G., and Dunker, A. M.: Modeling Weekday/Weekend Ozone Dif-
938 ferences in the Los Angeles Region for 1997, Journal of the Air & Waste Management Association, 53, 864–
939 875, doi:10.1080/10473289.2003.10466232, http://dx.doi.org/10.1080/10473289.2003.10466232, 2003.
940 Yarwood, G., Rao, S., Yocke, M., and Whitten, G. Z.: Updates to the Carbon Bond Chemical Mechanism:
941 CB05, Tech. rep., U. S Environmental Protection Agency, 2005.
942 Zaveri, R. A. and Peters, L. K.: A new lumped structure photochemical mechanism for large-scale applications,
943 Journal of Geophysical Research: Atmospheres, 104, 30 387–30 415, doi:10.1029/1999JD900876, http://dx.
944 doi.org/10.1029/1999JD900876, 1999.
945 Zhang, Y.: Online-coupled meteorology and chemistry models: history, current status, and outlook, Atmo-
946 spheric Chemistry and Physics, 8, 2895–2932, doi:10.5194/acp-8-2895-2008, http://www.atmos-chem-phys.
947 net/8/2895/2008/, 2008.
948 Zhang, Y., Pan, Y., Wang, K., Fast, J. D., and Grell, G. A.: WRF/Chem-MADRID: Incorporation of an aerosol
949 module into WRF/Chem and its initial application to the TexAQS2000 episode, Journal of Geophysical Re-
950 search: Atmospheres, 115, n/a–n/a, doi:10.1029/2009JD013443, http://dx.doi.org/10.1029/2009JD013443,
951 d18202, 2010.
952 Zhang, Y., Chen, Y., Sarwar, G., and Schere, K.: Impact of gas-phase mechanisms on Weather Research
953 Forecasting Model with Chemistry (WRF/Chem) predictions: Mechanism implementation and compara-
954 tive evaluation, Journal of Geophysical Research: Atmospheres, 117, n/a–n/a, doi:10.1029/2011JD015775,
955 http://dx.doi.org/10.1029/2011JD015775, d01301, 2012.
956 Zhang, Y., Sartelet, K., Wu, S.-Y., and Seigneur, C.: Application of WRFChem-MADRID and WRFPolyphemus
957 in Europe – Part 1: Model description, evaluation of meteorological predictions, and aerosol–meteorology
958 interactions, Atmospheric Chemistry and Physics, 13, 6807–6843, doi:10.5194/acp-13-6807-2013, http://
959 www.atmos-chem-phys.net/13/6807/2013/, 2013a.
960 Zhang, Y., Sartelet, K., Zhu, S., Wang, W., Wu, S.-Y., Zhang, X., Wang, K., Tran, P., Seigneur, C., and
961 Wang, Z.-F.: Application of WRF/Chem-MADRID and WRF/Polyphemus in Europe – Part 2: Evaluation of
962 chemical concentrations and sensitivity simulations, Atmospheric Chemistry and Physics, 13, 6845–6875,
963 doi:10.5194/acp-13-6845-2013, http://www.atmos-chem-phys.net/13/6845/2013/, 2013b.

Geosci. Model Dev. Discuss., doi:10.5194/gmd-2016-131, 2016
Manuscript under review for journal Geosci. Model Dev.
Published: 7 June 2016

Geoscientific Model Development Discussions
Open Access
EGU

Table 1. WRF-Chem options used in model simulations.

Atmospheric Process	Option used
Cloud microphysics	Lin et al. scheme (Lin et al., 1983)
Longwave radiation	RRTMG (Iacono et al., 2008)
Shortwave radiation	Goddard shortwave scheme (Chou and Suarez, 1994)
Surface Layer	MM5 Similarity based on Monin-Obukhov scheme (Beljaars, 1995)
Land-surface Physics	Noah Land Surface Model (Chen and Dudhia, 2001)
Urban surface physics	Urban Canopy Model (Kusaka and Kimura, 2004)
Planetary boundary layer	Yonsei University scheme (Hong et al., 2006)
Cumulus parametrization	Grell 3D scheme (Grell and Dévényi, 2002)

Table 2. Description of WRF-Chem simulations performed for this study.

	Simulation Name	Model Chemistry	Photolysis Scheme
(1)	MOZART	MOZART-4 chemistry with gocart aerosols, KPP solver	Madronich F-TUV photolysis
(2)	RADM2	RADM2 chemistry with MADE/SORGAM aerosols, KPP solver	Madronich photolysis (TUV)

Table 3. Observational datasets used for model evaluation.

Database	Parameter	Temporal Resolution	Data Source
BADC Global Weather Observation Data	MSLP, T2, WS10, WD10	3-hourly	http://badc.nerc.ac.uk/home/
AirBase v7	O_3, NO_2, NO, NO_x	hourly	http://www.eea.europa.eu/data-and-maps/data/airbase-the-european-air-quality-database-7
EMEP	NO_2, NO, NO_x	hourly	http://ebas.nilu.no/

Geosci. Model Dev. Discuss., doi:10.5194/gmd-2016-131, 2016
Manuscript under review for journal Geosci. Model Dev.
Published: 7 June 2016

Geoscientific Model Development Discussions
Open Access
EGU

Table 4. Domain-wide statistical performance of WRF-Chem against 3-hourly meteorological observations from BADC. Modeled quantities are from the MOZART simulation.

	Winter (DJF)							Spring (MAM)						
	Mean-Obs	Mean-Mod	MB	NMB	MFB	r	no. stations	Mean-Obs	Mean-Mod	MB	NMB	MFB	r	no. stations
MSLP (hPa)	1015.41	1014.79	-0.96	0.00	0.00	0.99	1297	1014.67	1014.46	-0.35	0.00	0.00	0.99	1295
T2 (° C)	2.51	2.99	0.29	0.11	-0.01	0.89	1581	9.73	9.91	-0.11	-0.01	0.07	0.94	1581
WS10 (m/s)	4.31	5.60	1.34	0.31	0.42	0.71	1577	3.86	4.46	0.65	0.17	0.29	0.68	1589
WD10 (deg)	175.53	203.73	27.93	0.16	0.27	0.50	1568	167.88	188.67	21.16	0.13	0.25	0.48	1580
	Summer (JJA)							Fall (SON)						
	Mean-Obs	Mean-Mod	MB	NMB	MFB	r	no. stations	Mean-Obs	Mean-Mod	MB	NMB	MFB	r	no. stations
MSLP (hPa)	1012.12	1012.11	0.04	0.00	0.00	0.98	1288	1017.61	1017.42	-0.49	0.00	0.00	0.99	1297
T2 (° C)	17.82	17.70	-0.38	-0.02	0.00	0.87	1573	9.20	9.65	0.24	0.03	-0.08	0.95	1583
WS10 (m/s)	3.45	3.90	0.48	0.14	0.27	0.63	1574	3.64	4.61	1.04	0.28	0.40	0.68	1585
WD10 (deg)	173.88	196.92	23.27	0.13	0.25	0.45	1561	172.30	196.49	24.02	0.14	0.27	0.48	1574

Geosci. Model Dev. Discuss., doi:10.5194/gmd-2016-131, 2016
Manuscript under review for journal Geosci. Model Dev.
Published: 7 June 2016

Geoscientific Model Development Discussions
Open Access
EGU

Table 5. Statistics for MOZART simulation against hourly observations from the AirBase network. Means and MB are expressed in $\mu g\,m^{-3}$; NMB, MFB, and r are unitless. r is the hourly temporal correlation coefficient for all quantities except MDA8, for which it represents the daily temporal correlation coefficient.

	Winter (DJF)							Spring (MAM)						
	Mean-Obs	Mean-Mod	MB	NMB	MFB	r	no. stations	Mean-Obs	Mean-Mod	MB	NMB	MFB	r	no. stations
O_3	53.82	48.34	-5.44	-0.10	-0.10	0.60	366	75.26	70.93	-4.25	-0.06	-0.07	0.56	371
MDA8	67.50	64.20	-3.30	-0.05	-0.04	0.76	365	96.33	97.00	0.67	0.01	0.00	0.69	370
NO_x	20.22	16.99	-3.20	-0.16	0.00	0.37	204	14.30	13.32	-0.99	-0.07	-0.15	0.25	210
NO_2	14.40	14.83	0.48	0.03	0.07	0.42	250	11.34	12.03	0.70	0.06	-0.10	0.30	252
NO	4.27	1.18	-3.10	-0.73	-1.24	0.29	148	2.65	0.79	-1.87	-0.70	-1.26	0.27	148
	Summer (JJA)							Fall (SON)						
	Mean-Obs	Mean-Mod	MB	NMB	MFB	r	no. stations	Mean-Obs	Mean-Mod	MB	NMB	MFB	r	no. stations
O_3	70.84	80.72	9.92	0.14	0.14	0.55	370	47.24	53.10	6.14	0.13	0.13	0.57	367
MDA8	94.51	110.37	15.86	0.17	0.16	0.61	369	63.81	74.82	11.01	0.17	0.15	0.65	367
NO_x	10.63	10.57	-0.10	-0.01	-0.21	0.16	206	19.14	16.62	-2.53	-0.13	-0.07	0.32	208
NO_2	8.30	9.66	1.37	0.17	-0.12	0.22	248	13.60	15.23	1.64	0.12	0.05	0.38	253
NO	2.01	0.48	-1.53	-0.76	-1.36	0.19	148	4.24	1.07	-3.17	-0.75	-1.32	0.28	146

Geosci. Model Dev. Discuss., doi:10.5194/gmd-2016-131, 2016
Manuscript under review for journal Geosci. Model Dev.
Published: 7 June 2016

Geoscientific Model Development Discussions
Open Access
EGU

Table 6. Statistics for MOZART simulation against hourly observations from the EMEP network. Means and MB are expressed in $\mu g\,m^{-3}$; NMB, MFB, and r are unitless. r is the hourly temporal correlation coefficient for all quantities except MDA8, for which it represents the daily temporal correlation coefficient.

	Winter (DJF)							Spring (MAM)						
	Mean-Obs	Mean-Mod	MB	NMB	MFB	r	no. stations	Mean-Obs	Mean-Mod	MB	NMB	MFB	r	no. stations
O_3	54.54	43.82	-10.46	-0.19	-0.22	0.53	118	78.99	68.62	-10.53	-0.13	-0.16	0.55	120
MDA8	64.66	55.09	-9.57	-0.15	-0.16	0.56	117	95.64	90.15	-5.49	-0.06	-0.07	0.65	119
NO_x	11.36	12.39	1.10	0.10	0.18	0.42	8	10.21	10.44	0.41	0.04	-0.04	0.33	9
NO_2	10.19	13.24	3.09	0.30	0.25	0.53	34	8.07	10.72	2.55	0.32	-0.01	0.37	38
NO	2.10	1.22	-0.87	-0.41	-0.65	0.36	25	1.34	0.78	-0.56	-0.42	-0.50	0.35	27
	Summer (JJA)							Fall (SON)						
	Mean-Obs	Mean-Mod	MB	NMB	MFB	r	no. stations	Mean-Obs	Mean-Mod	MB	NMB	MFB	r	no. stations
O_3	72.08	76.39	4.04	0.06	0.06	0.54	120	53.24	52.05	-1.08	-0.02	-0.02	0.54	122
MDA8	91.24	101.48	10.24	0.11	0.11	0.59	119	66.99	70.37	3.39	0.05	0.04	0.57	121
NO_x	7.62	8.44	0.94	0.12	-0.12	0.30	9	11.83	12.14	0.76	0.06	0.03	0.34	9
NO_2	6.07	9.10	2.96	0.49	0.06	0.30	38	8.88	13.81	5.08	0.57	0.23	0.40	38
NO	1.23	0.60	-0.64	-0.52	-0.52	0.28	29	1.42	1.23	-0.14	-0.10	-0.36	0.34	28

Table 7. Statistics for yearly SOMO35 in $mg\,m^{-3} \cdot days$.

Simulation	Observation network	Obs	Model	MB	NMB	MFB	no. stations
MOZART	AirBase	6.23	8.22	1.98	0.32	0.30	375
MOZART	EMEP	5.73	6.27	0.51	0.09	0.11	122
RADM2	AirBase	6.23	2.55	-3.68	-0.59	-0.87	375
RADM2	EMEP	5.73	1.84	-3.91	-0.68	-1.13	122

Geosci. Model Dev. Discuss., doi:10.5194/gmd-2016-131, 2016
Manuscript under review for journal Geosci. Model Dev.
Published: 7 June 2016

Geoscientific Model Development Discussions
Open Access
EGU

Table 8. Statistics for RADM2 simulation against hourly observations from the AirBase network. Means and MB are expressed in $\mu g\,m^{-3}$; NMB, MFB, and r are unitless. r is the hourly temporal correlation coefficient for all quantities except MDA8, for which it represents the daily temporal correlation coefficient.

	Winter (DJF)							Spring (MAM)						
	Mean-Obs	Mean-Mod	MB	NMB	MFB	r	no. stations	Mean-Obs	Mean-Mod	MB	NMB	MFB	r	no. stations
O_3	53.82	41.57	-12.18	-0.23	-0.25	0.60	366	75.26	53.36	-21.81	-0.29	-0.33	0.53	371
MDA8	67.50	56.04	-11.46	-0.17	-0.17	0.75	365	96.33	74.73	-21.60	-0.22	-0.25	0.67	370
NO_x	20.22	13.75	-6.45	-0.32	-0.23	0.36	204	14.30	11.44	-2.87	-0.20	-0.32	0.21	210
NO_2	14.40	11.90	-2.47	-0.17	-0.15	0.41	250	11.34	10.31	-1.01	-0.09	-0.27	0.27	252
NO	4.27	0.97	-3.31	-0.77	-1.34	0.27	148	2.65	0.67	-1.99	-0.75	-1.34	0.26	148
	Summer (JJA)							Fall (SON)						
	Mean-Obs	Mean-Mod	MB	NMB	MFB	r	no. stations	Mean-Obs	Mean-Mod	MB	NMB	MFB	r	no. stations
O_3	70.84	57.79	-13.01	-0.18	-0.18	0.58	370	47.24	39.00	-8.03	-0.17	-0.18	0.59	367
MDA8	94.51	80.59	-13.92	-0.15	-0.15	0.71	369	63.81	56.02	-7.79	-0.12	-0.12	0.69	367
NO_x	10.63	9.79	-0.87	-0.08	-0.29	0.14	206	19.14	14.30	-4.84	-0.25	-0.24	0.30	208
NO_2	8.30	8.95	0.67	0.08	-0.19	0.21	248	13.60	12.57	-1.01	-0.07	-0.13	0.36	253
NO	2.01	0.46	-1.55	-0.77	-1.42	0.18	148	4.24	1.28	-2.97	-0.70	-1.27	0.26	146

Geosci. Model Dev. Discuss., doi:10.5194/gmd-2016-131, 2016
Manuscript under review for journal Geosci. Model Dev.
Published: 7 June 2016

Geoscientific Model Development Discussions
Open Access
EGU

Table 9. Statistics for RADM2 simulation against hourly observations from the EMEP network. Means and MB are expressed in $\mu g\,m^{-3}$; NMB, MFB, and r are unitless. r is the hourly temporal correlation coefficient for all quantities except MDA8, for which it represents the daily temporal correlation coefficient.

	Winter (DJF)							Spring (MAM)						
	Mean-Obs	Mean-Mod	MB	NMB	MFB	r	no. stations	Mean-Obs	Mean-Mod	MB	NMB	MFB	r	no. stations
O_3	54.54	38.67	-15.62	-0.29	-0.36	0.54	118	78.99	53.24	-25.83	-0.33	-0.40	0.49	120
MDA8	64.66	49.40	-15.26	-0.24	-0.27	0.56	117	95.64	71.04	-24.60	-0.26	-0.29	0.55	119
NO_x	11.36	10.31	-0.99	-0.09	-0.02	0.38	8	10.21	8.76	-1.31	-0.13	-0.24	0.30	9
NO_2	10.19	10.72	0.56	0.06	0.03	0.51	34	8.07	9.11	0.95	0.12	-0.19	0.34	38
NO	2.10	1.16	-0.93	-0.44	-0.67	0.37	25	1.34	0.68	-0.67	-0.50	-0.59	0.31	27
	Summer (JJA)							Fall (SON)						
	Mean-Obs	Mean-Mod	MB	NMB	MFB	r	no. stations	Mean-Obs	Mean-Mod	MB	NMB	MFB	r	no. stations
O_3	72.08	55.65	-16.65	-0.23	-0.24	0.58	120	53.24	39.89	-13.21	-0.25	-0.29	0.57	122
MDA8	91.24	74.75	-16.49	-0.18	-0.19	0.69	119	66.99	54.31	-12.68	-0.19	-0.21	0.63	121
NO_x	7.62	7.61	0.10	0.01	-0.24	0.28	9	11.83	10.59	-0.82	-0.07	-0.13	0.32	9
NO_2	6.07	8.33	2.20	0.36	-0.02	0.29	38	8.88	11.48	2.71	0.31	0.04	0.39	38
NO	1.23	0.52	-0.73	-0.59	-0.58	0.25	29	1.42	1.43	0.07	0.05	-0.31	0.31	28

Geosci. Model Dev. Discuss., doi:10.5194/gmd-2016-131, 2016
Manuscript under review for journal Geosci. Model Dev.
Published: 7 June 2016

Geoscientific Model Development Discussions
Open Access
EGU

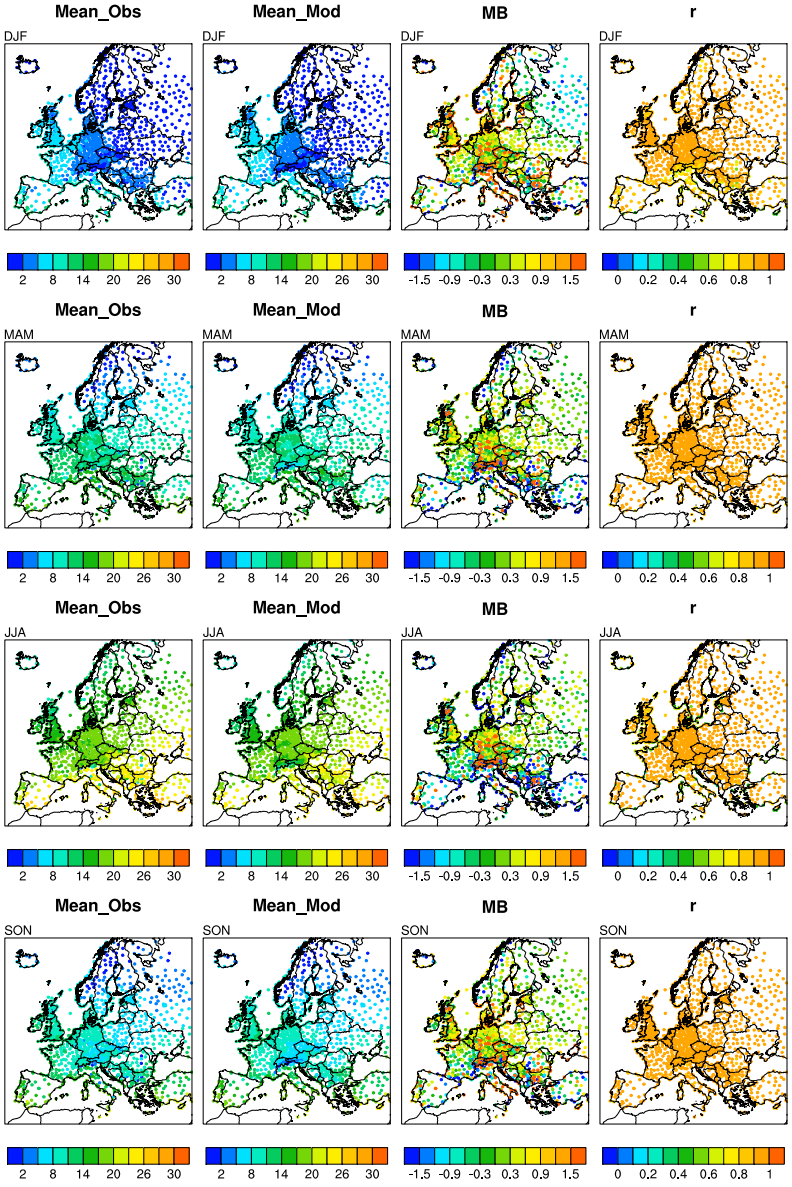

Figure 1. Seasonal average values of 2-meter temperature (T2) in degrees Celcius. Model results and statistics are shown for the MOZART simulation at the locations of the observations.

Geosci. Model Dev. Discuss., doi:10.5194/gmd-2016-131, 2016
Manuscript under review for journal Geosci. Model Dev.
Published: 7 June 2016

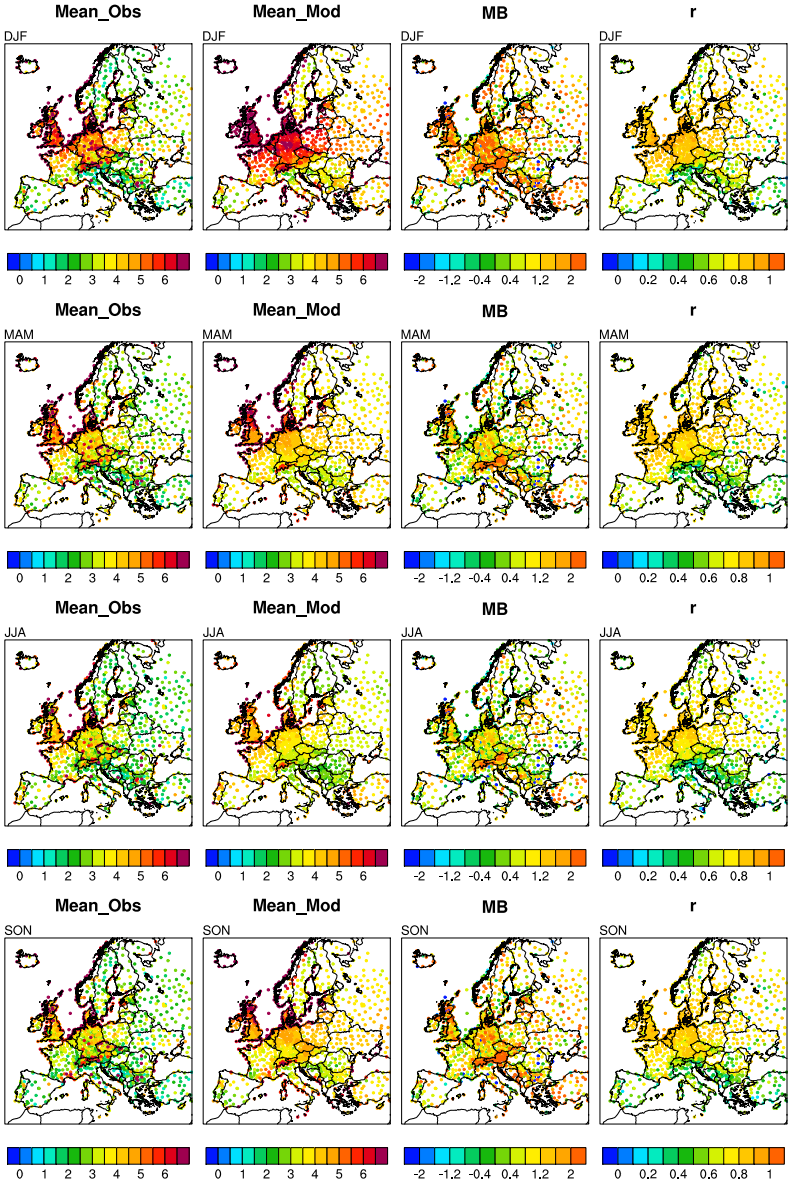

Figure 2. Seasonal average values of 10-meter wind speed (WS10) in $\mathrm{m/s}$. Model results and statistics are shown for the MOZART simulation at the locations of the observations.

Geosci. Model Dev. Discuss., doi:10.5194/gmd-2016-131, 2016
Manuscript under review for journal Geosci. Model Dev.
Published: 7 June 2016

Geoscientific Model Development Discussions
Open Access
EGU

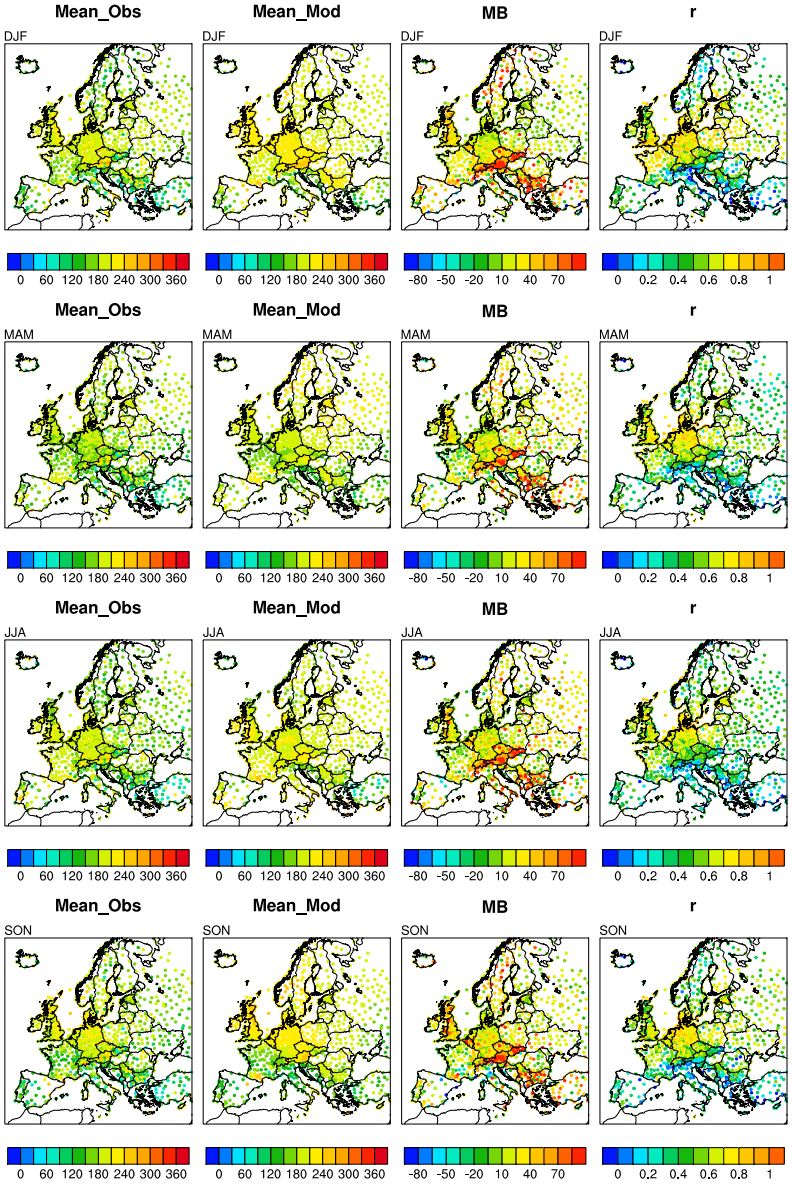

Figure 3. Seasonal average values of 10-meter wind speed (WS10) in $\mathrm{m/s}$. Model results and statistics are shown for the MOZART simulation at the locations of the observations.

Geosci. Model Dev. Discuss., doi:10.5194/gmd-2016-131, 2016
Manuscript under review for journal Geosci. Model Dev.
Published: 7 June 2016

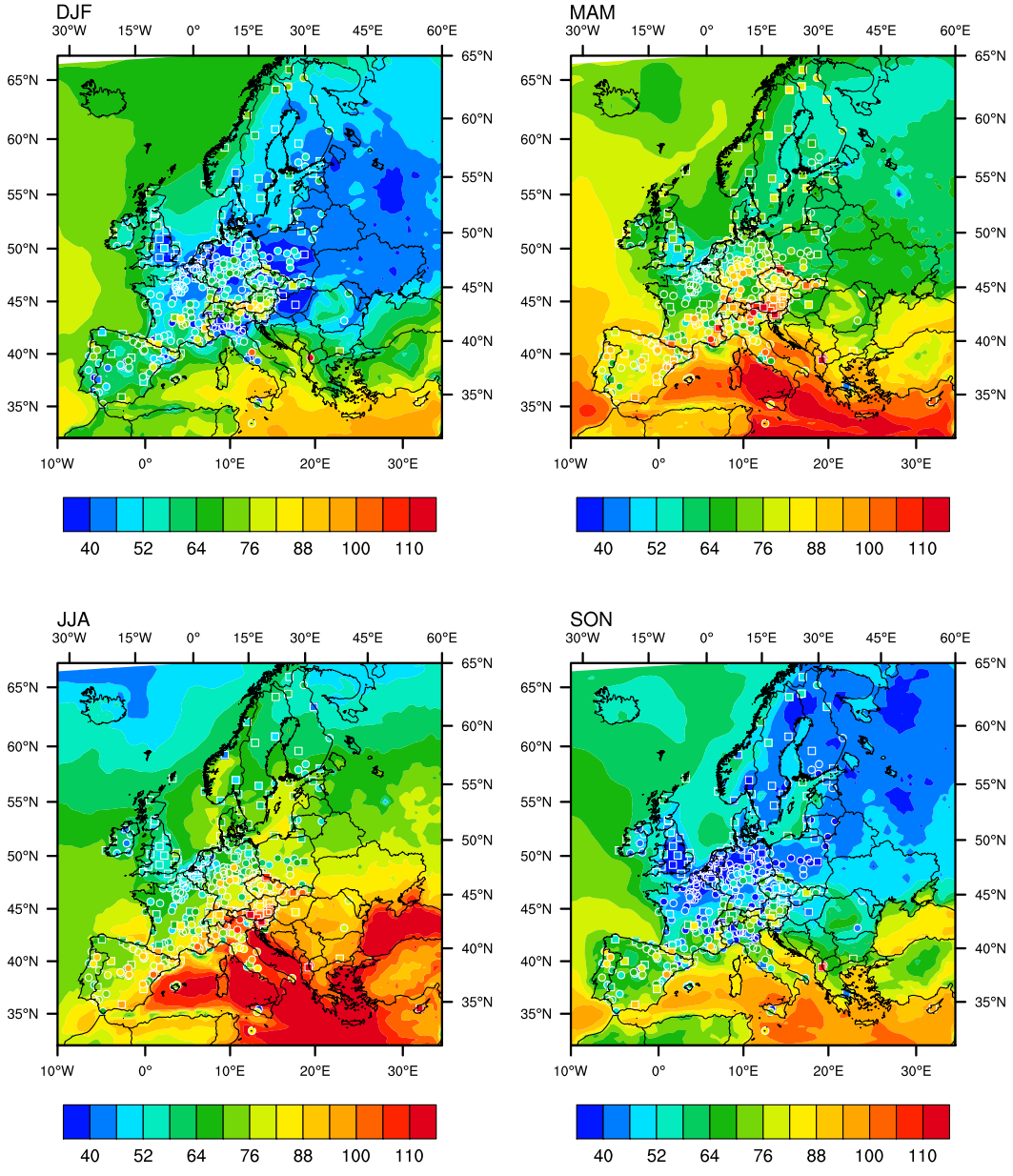

Figure 4. Seasonal average values of surface O_3 in $\mu g\,m^{-3}$. Contours are model output from the MOZART simulation. Filled dots represent hourly measurements at AirBase rural background stations, filled squares represent measurements at EMEP stations.

Geosci. Model Dev. Discuss., doi:10.5194/gmd-2016-131, 2016
Manuscript under review for journal Geosci. Model Dev.
Published: 7 June 2016

Geoscientific Model Development Discussions
Open Access
EGU

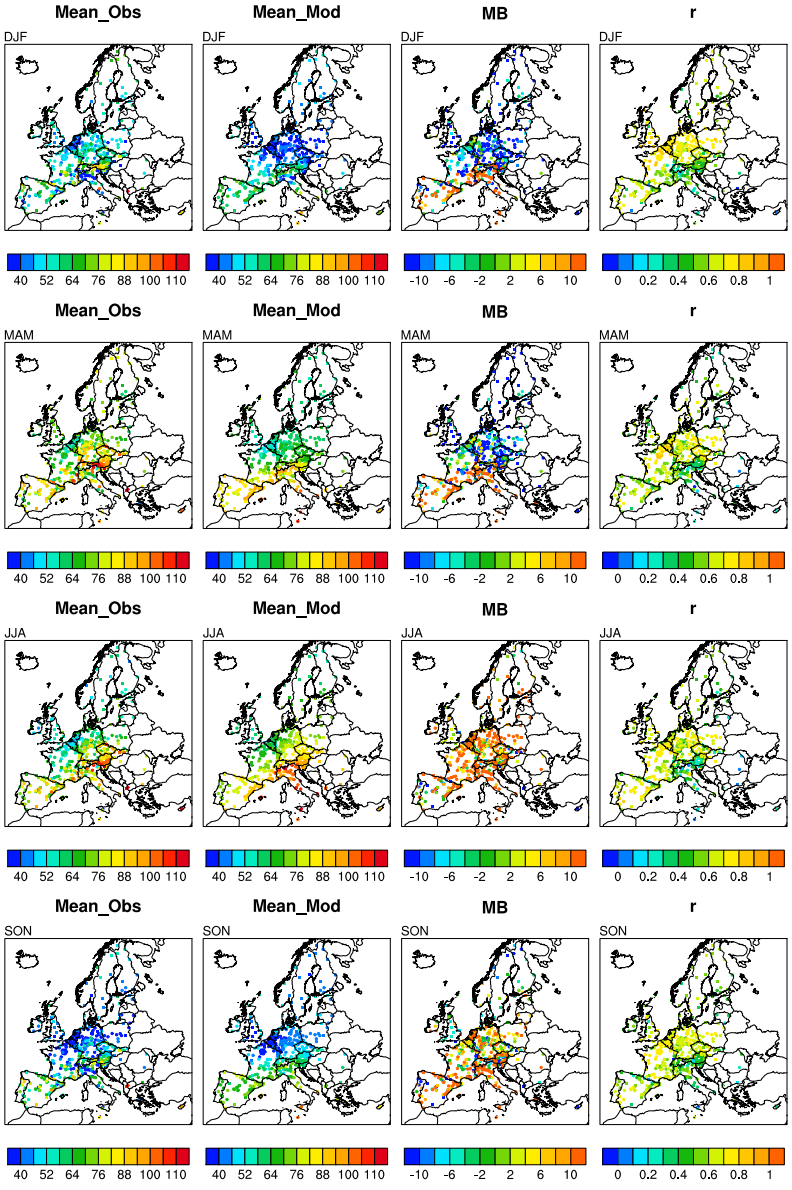

Figure 5. Seasonal average values of surface O_3 in $\mu g\,m^{-3}$ from hourly measurements at AirBase (circles) and EMEP (squares) stations, and modeled values from MOZART for corresponding locations. The Mean Bias (MB, in $\mu g\,m^{-3}$) and temporal correlation coefficient (r) for hourly values are also shown at the location of station observations.

Geosci. Model Dev. Discuss., doi:10.5194/gmd-2016-131, 2016
Manuscript under review for journal Geosci. Model Dev.
Published: 7 June 2016

Geoscientific Model Development Discussions
Open Access
EGU

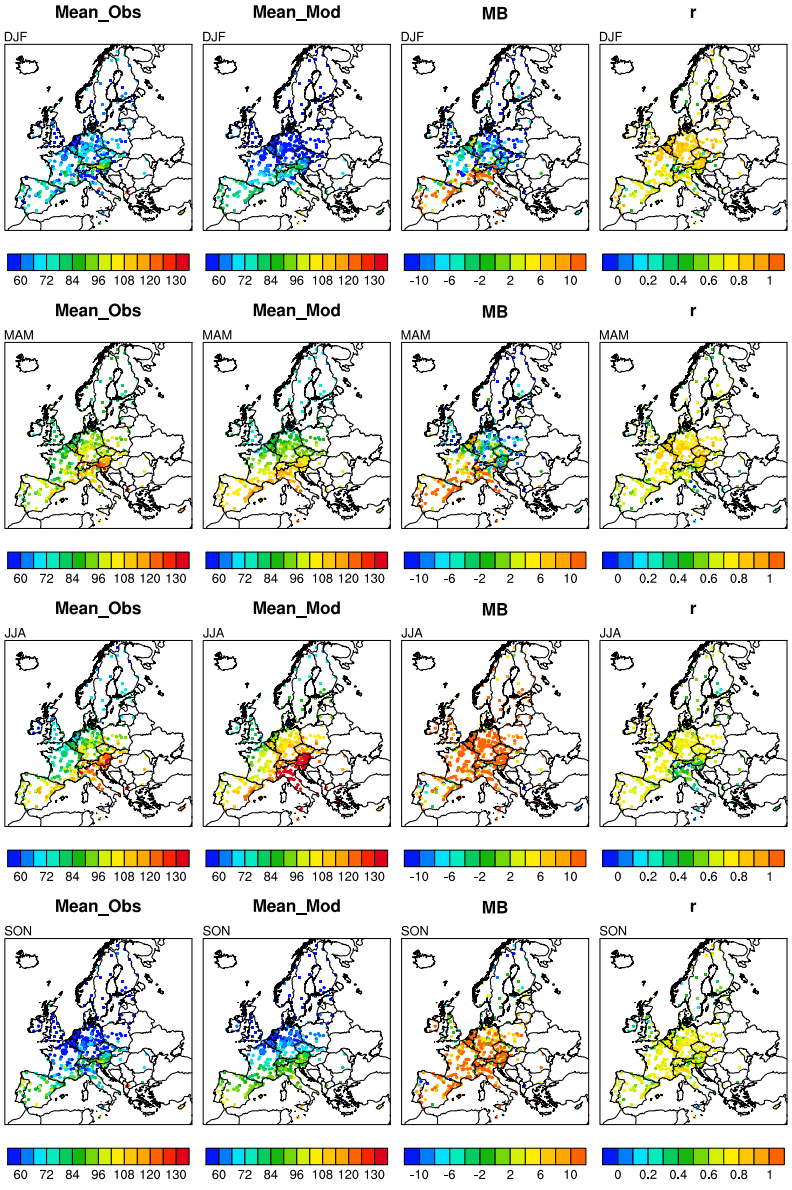

Figure 6. Seasonal average values of MDA8 in $\mu g\,m^{-3}$ calculated from hourly measurements at AirBase (circles) and EMEP (squares) stations, and modeled values from MOZART for corresponding locations. The Mean Bias (MB, in $\mu g\,m^{-3}$) and temporal correlation coefficient (r) for daily values are also shown at the location of station observations.

Geosci. Model Dev. Discuss., doi:10.5194/gmd-2016-131, 2016
Manuscript under review for journal Geosci. Model Dev.
Published: 7 June 2016

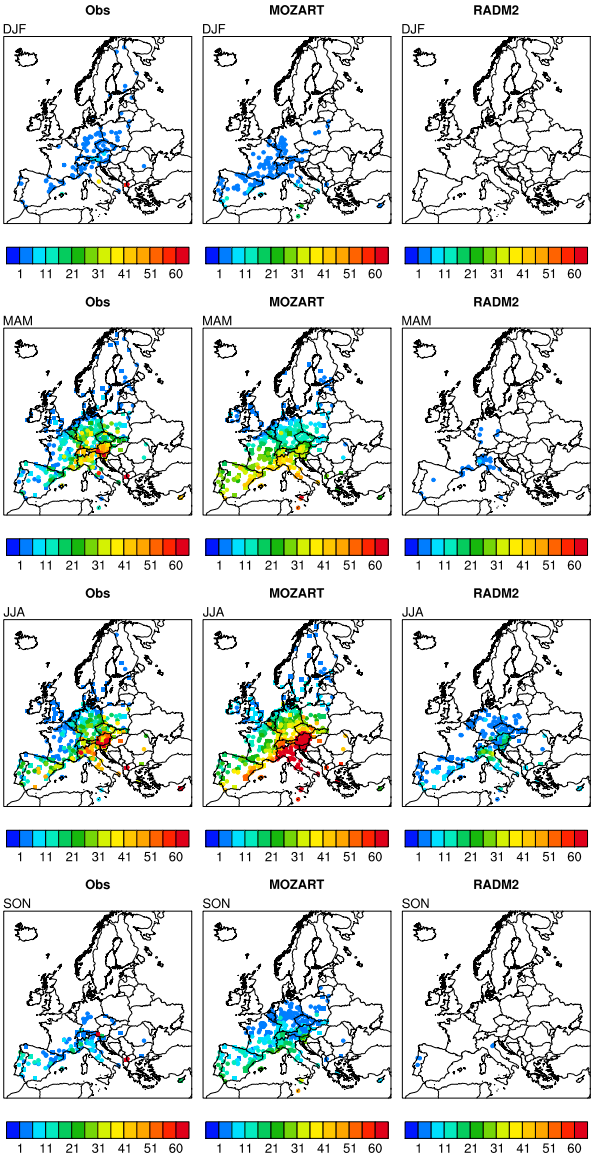

Figure 7. Number of days of exceedances of the EU long-term objective value for MDA8 (120 $\mu g\,m^{-3}$) at AirBase (circles) and EMEP (squares) station locations. Shown are totals by season for observations and the MOZART and RADM2 simulations. For simplicity of viewing the data, stations with no exceedances are not plotted.

Geosci. Model Dev. Discuss., doi:10.5194/gmd-2016-131, 2016
Manuscript under review for journal Geosci. Model Dev.
Published: 7 June 2016

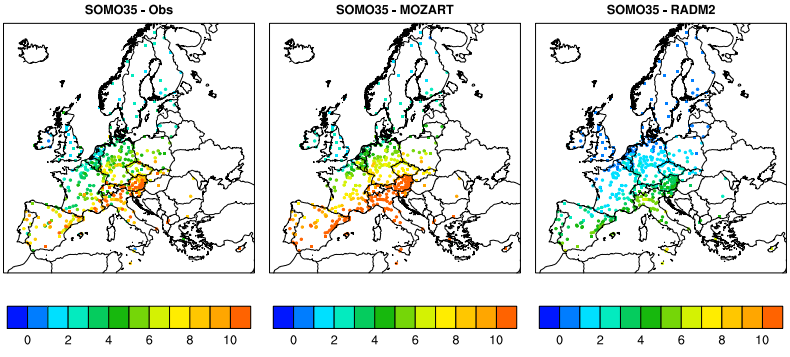

Figure 8. Yearly values of SOMO35 in $\mathrm{mg\,m^{-3}\cdot days}$ calculated from hourly measurements at AirBase (circles) and EMEP (squares) stations, and modeled values for corresponding locations.

Geosci. Model Dev. Discuss., doi:10.5194/gmd-2016-131, 2016
Manuscript under review for journal Geosci. Model Dev.
Published: 7 June 2016

Geoscientific Model Development Discussions
Open Access
EGU

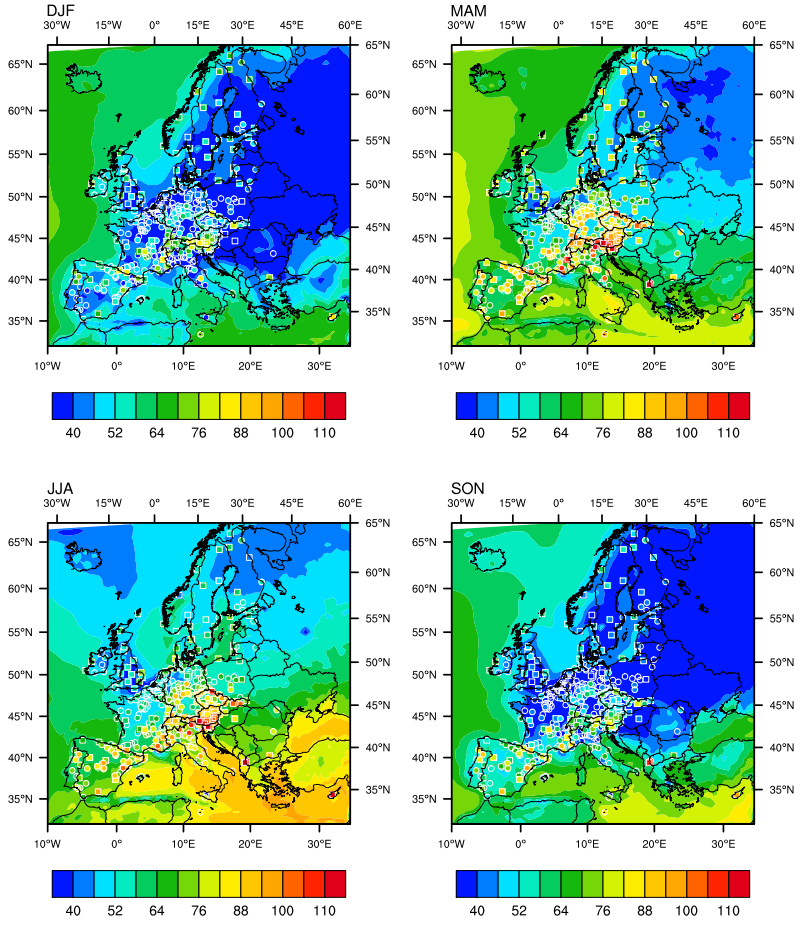

Figure 9. Seasonal average values of surface O_3 in $\mu g\ m^{-3}$. Contours are model output from the RADM2 simulation. Filled dots represent hourly measurements at AirBase rural background stations, filled squares represent measurements at EMEP stations.

Geosci. Model Dev. Discuss., doi:10.5194/gmd-2016-131, 2016
Manuscript under review for journal Geosci. Model Dev.
Published: 7 June 2016

Geoscientific Model Development Discussions
Open Access
EGU

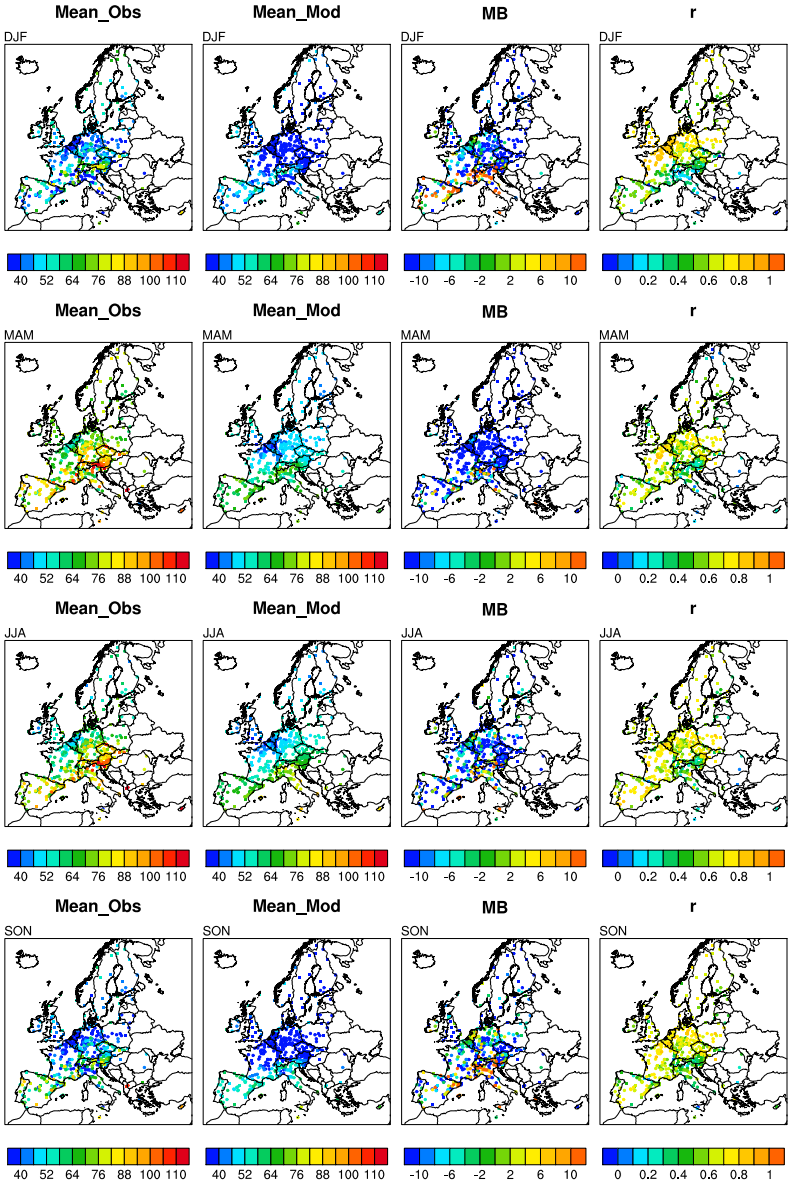

Figure 10. Seasonal average values of surface O_3 in $\mu g\,m^{-3}$ from hourly measurements at AirBase (circles) and EMEP (squares) stations, and modeled values from RADM2 for corresponding locations. The Mean Bias (MB, in $\mu g\,m^{-3}$) and temporal correlation coefficient (r) for hourly values are also shown at the location of station observations.

Geosci. Model Dev. Discuss., doi:10.5194/gmd-2016-131, 2016
Manuscript under review for journal Geosci. Model Dev.
Published: 7 June 2016

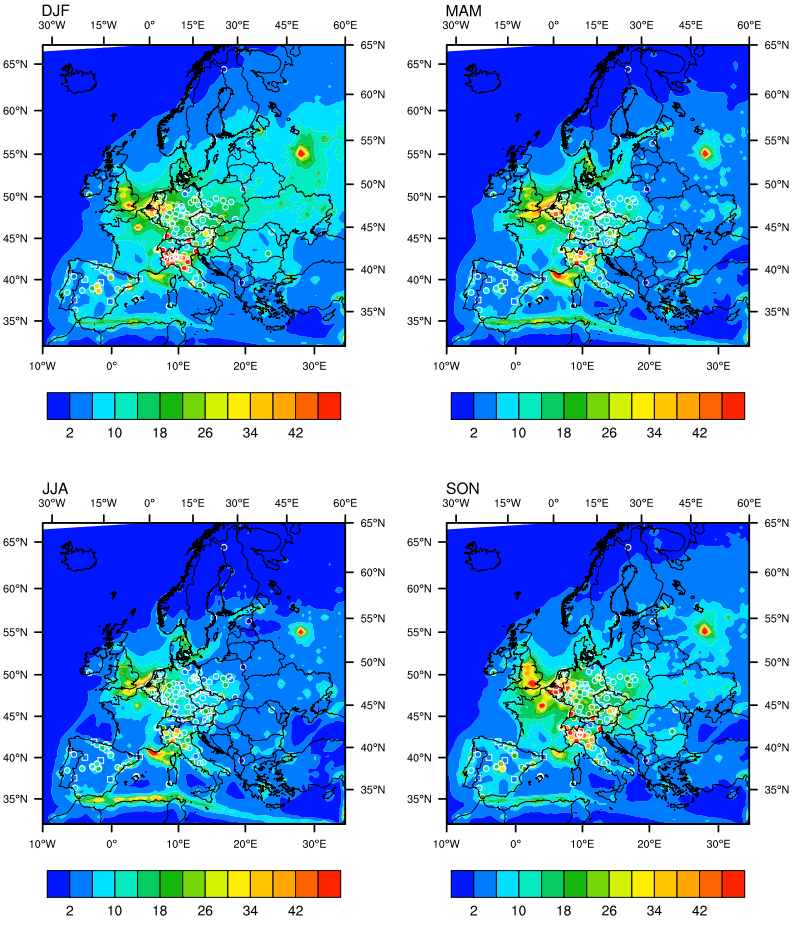

Figure 11. Seasonal average values of surface NO_x in $\mu g\ m^{-3}$. Contours are model output from the MOZART simulation. Filled dots represent hourly measurements at AirBase rural background stations, filled squares represent measurements at EMEP stations.

Geosci. Model Dev. Discuss., doi:10.5194/gmd-2016-131, 2016
Manuscript under review for journal Geosci. Model Dev.
Published: 7 June 2016

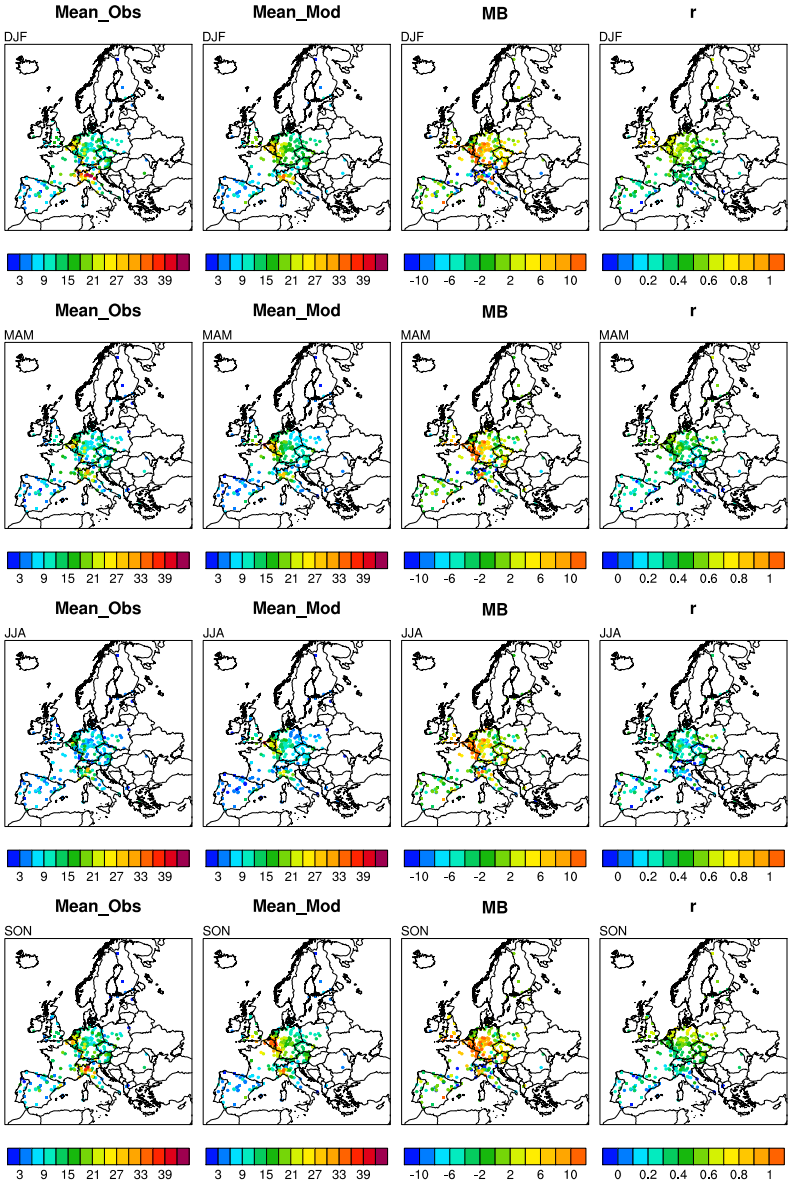

Figure 12. Seasonal average values of surface NO_2 in $\mu g\,m^{-3}$ from hourly measurements at AirBase (circles) and EMEP (squares) stations, and modeled values from MOZART for corresponding locations. The Mean Bias (MB) and temporal correlation coefficient (r) for hourly values are also shown at the location of station observations.

Geosci. Model Dev. Discuss., doi:10.5194/gmd-2016-131, 2016
Manuscript under review for journal Geosci. Model Dev.
Published: 7 June 2016

Geoscientific Model Development Discussions
Open Access
EGU

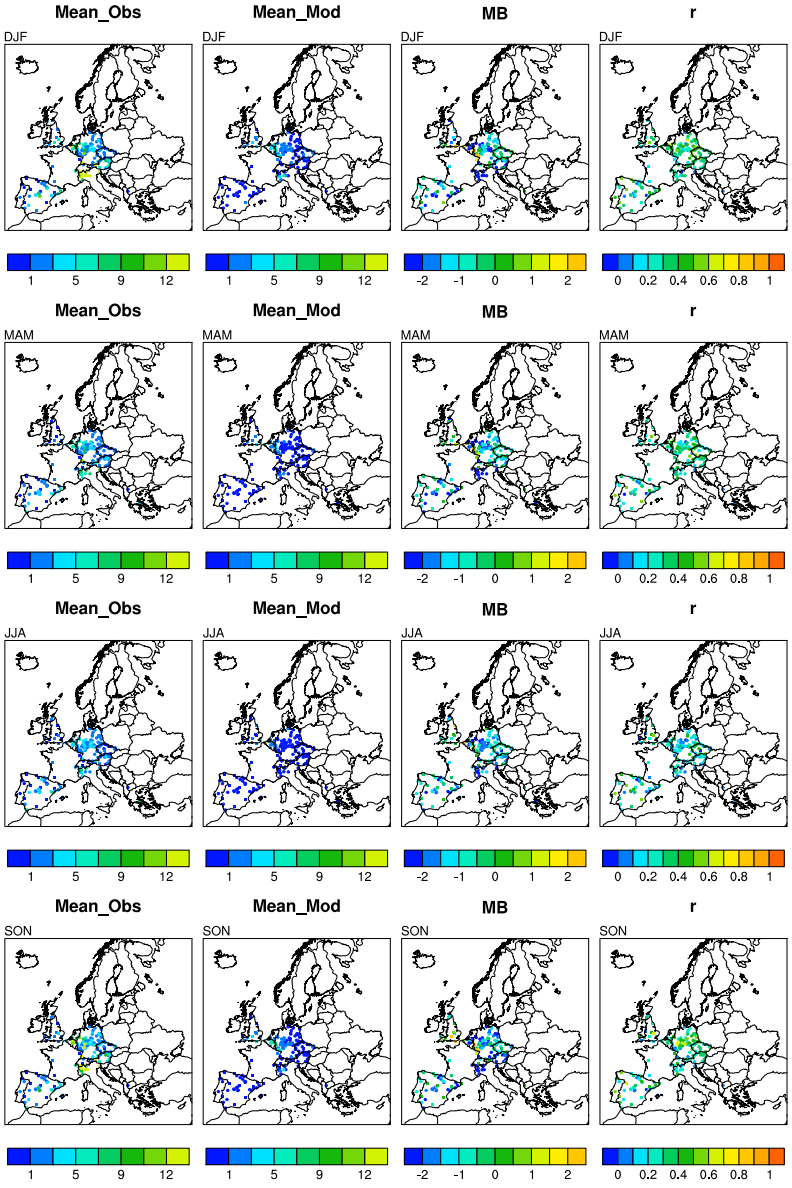

Figure 13. Seasonal average values of surface NO in $\mu g\,m^{-3}$ from hourly measurements at AirBase (circles) and EMEP (squares) stations, and modeled values from MOZART for corresponding locations. The Mean Bias (MB) and temporal correlation coefficient (r) for hourly values are also shown at the location of station observations.

Geosci. Model Dev. Discuss., doi:10.5194/gmd-2016-131, 2016
Manuscript under review for journal Geosci. Model Dev.
Published: 7 June 2016

Geoscientific Model Development Discussions
Open Access
EGU

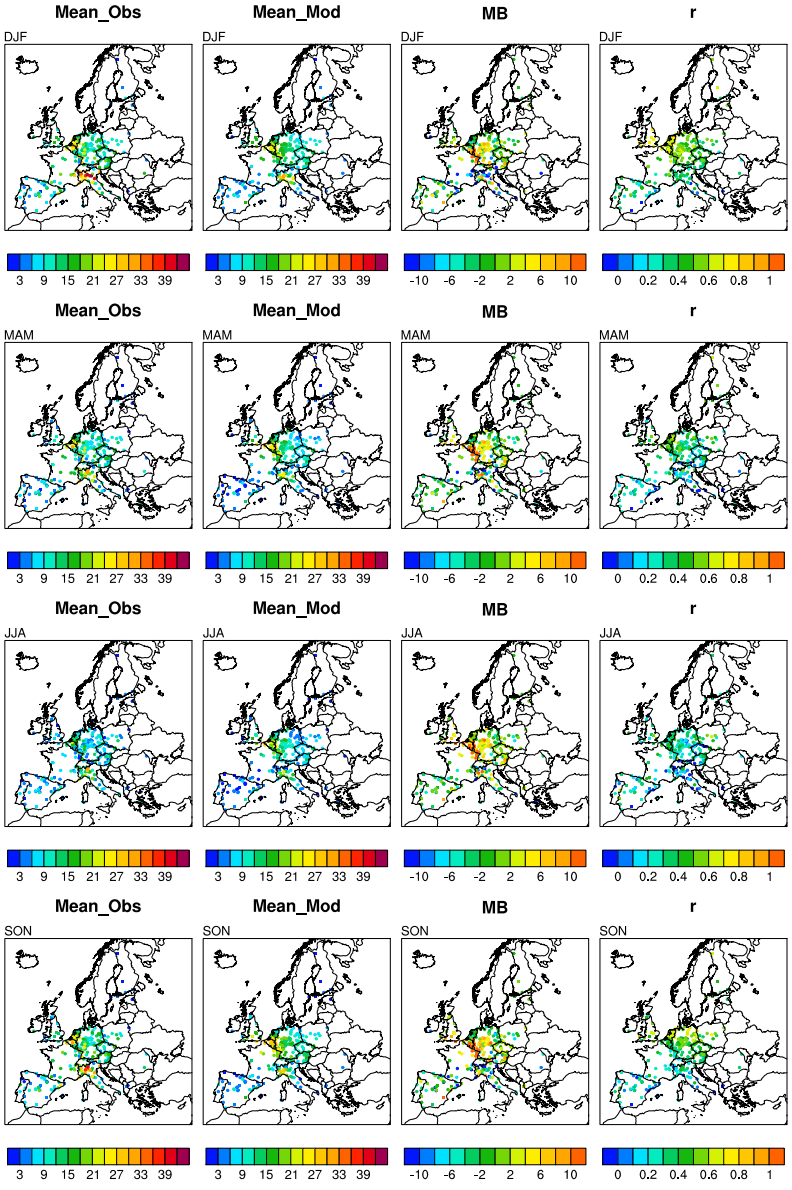

Figure 14. Seasonal average values of surface NO_2 in $\mu g\,m^{-3}$ from hourly measurements at AirBase (circles) and EMEP (squares) stations, and modeled values from RADM2 for corresponding locations. The Mean Bias (MB) and temporal correlation coefficient (r) for hourly values are also shown at the location of station observations.

Geosci. Model Dev. Discuss., doi:10.5194/gmd-2016-131, 2016
Manuscript under review for journal Geosci. Model Dev.
Published: 7 June 2016

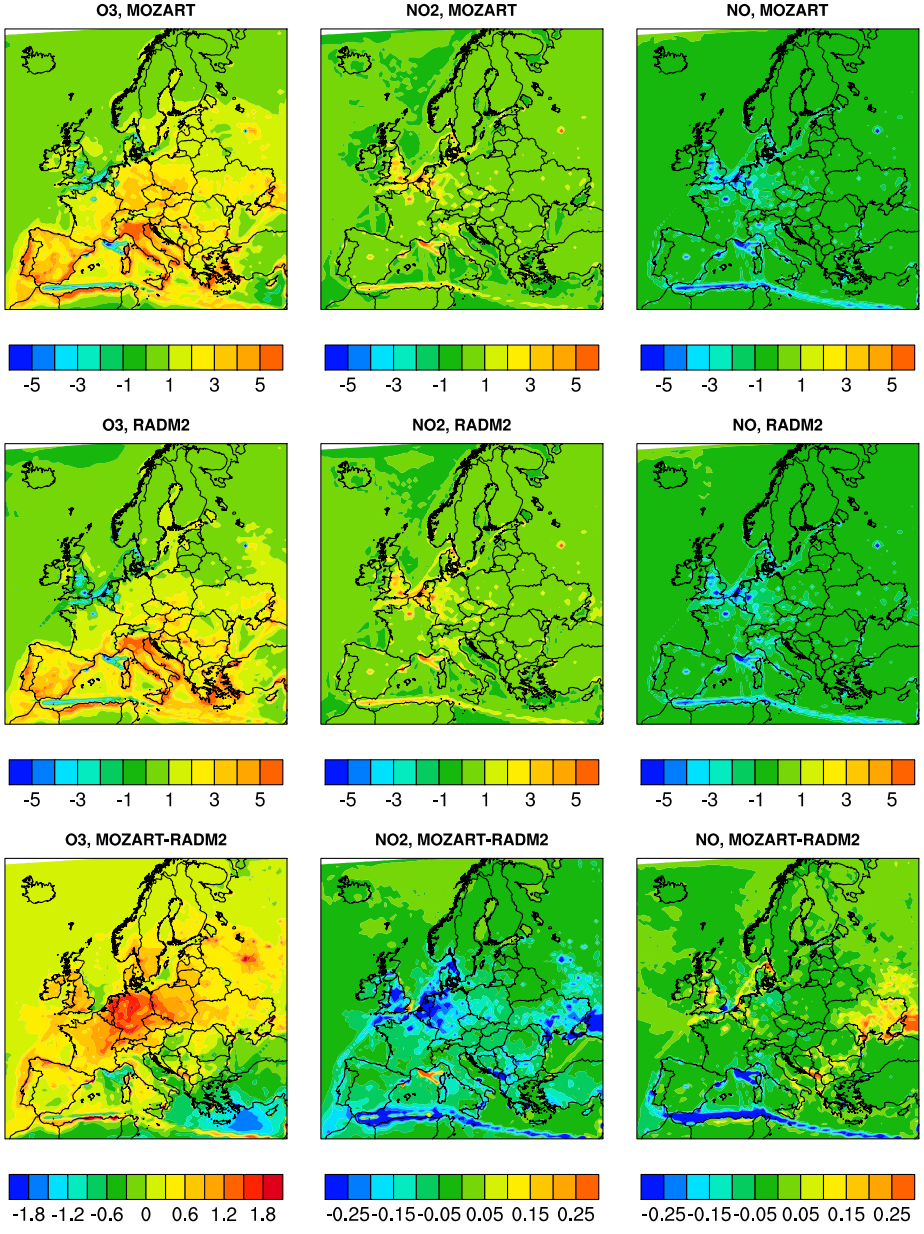

Figure 15. Net midday (11:00 - 14:00 CEST) photochemical production rate in $\mathrm{ppb\,hr^{-1}}$ for O_3, NO_2, and NO shown for MOZART and RADM2 for July 2007. The last row shows the difference in net production rate in $\mathrm{ppb\,hr^{-1}}$ (RADM2 subtracted from MOZART).

Geosci. Model Dev. Discuss., doi:10.5194/gmd-2016-131, 2016
Manuscript under review for journal Geosci. Model Dev.
Published: 7 June 2016

Geoscientific Model Development Discussions
Open Access
EGU

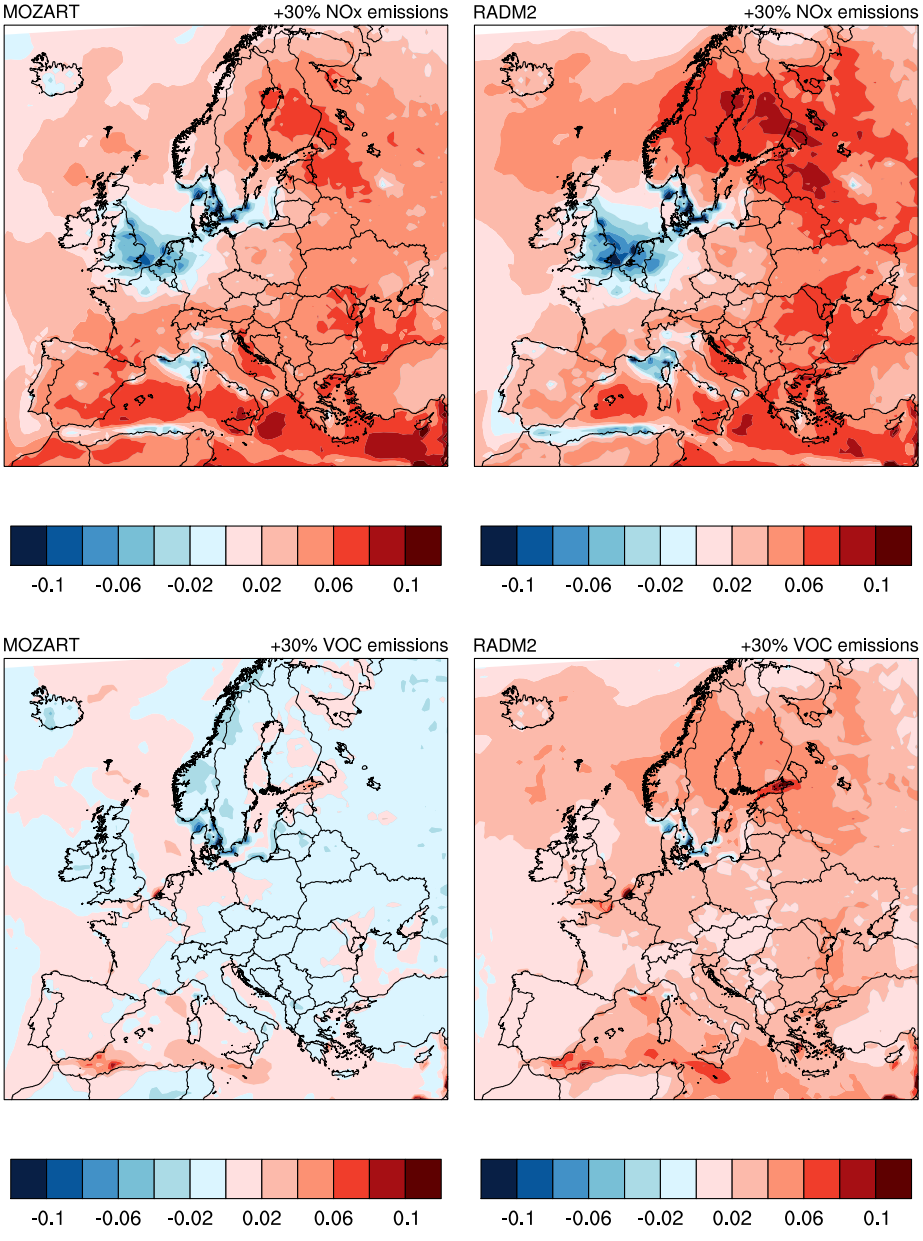

Figure 16. Sensitivity of average O_3 for July 2007 to a 30% increase in emissions of NO_x (upper row) or VOC (lower row), shown for the MOZART and RADM2 chemical mechanisms. Shown here is the fractional change in O_3 concentration, i.e., $([O3]_{+30\%emissions}\text{-}[O3]_{base})/[O3]_{base}$.